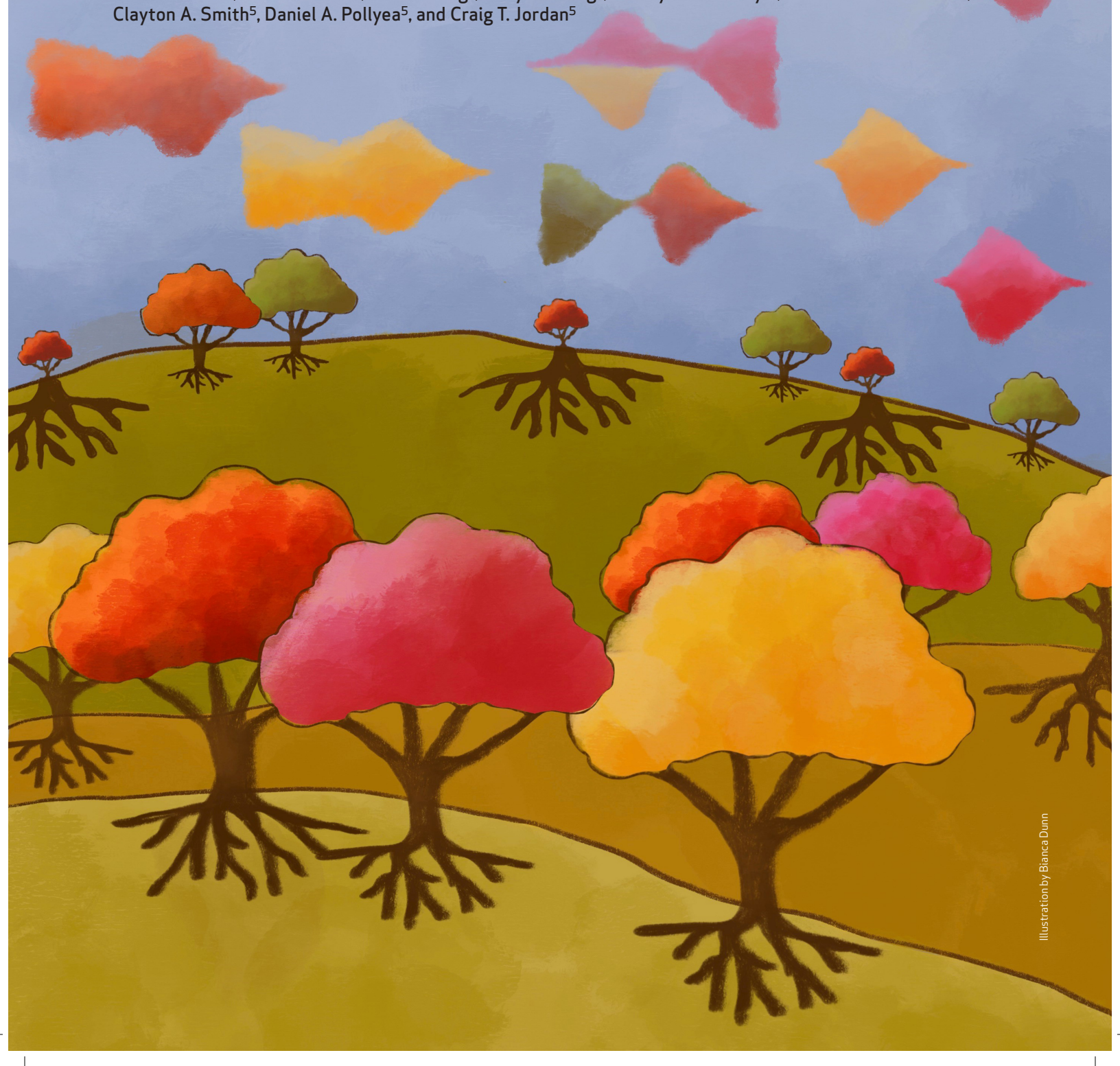




Shanshan Pei<sup>1,2,3,4</sup>, Ian T. Shelton<sup>5</sup>, Austin E. Gillen<sup>5,6</sup>, Brett M. Stevens<sup>5</sup>, Maura Gasparetto<sup>5</sup>, Yanan Wang<sup>1,2,3,4</sup>, Lina Liu<sup>1,2,3,4</sup>, Jun Liu<sup>1,2,3,4</sup>, Tonya M. Brunetti<sup>7,8</sup>, Krysta Engel<sup>5</sup>, Sarah Staggs<sup>5</sup>, William Showers<sup>5</sup>, Anagha Inguva Sheth<sup>5</sup>, Maria L. Amaya<sup>5,6</sup>, Mohammad Minhajuddin<sup>5</sup>, Amanda Winters<sup>9</sup>, Sweta B. Patel<sup>5</sup>, Hunter Tolison<sup>5</sup>, Anna E. Krug<sup>5</sup>, Tracy N. Young<sup>5</sup>, Jeffrey Schowinsky<sup>10</sup>, Christine M. McMahon<sup>5</sup>, Clayton A. Smith<sup>5</sup>, Daniel A. Pollyea<sup>5</sup>, and Craig T. Jordan<sup>5</sup>



**ABSTRACT** 

The BCL2 inhibitor venetoclax has recently emerged as an important component of acute myeloid leukemia (AML) therapy. Notably, use of this agent has revealed a pre-

viously unrecognized form of pathogenesis characterized by monocytic disease progression. We demonstrate that this form of disease arises from a fundamentally different type of leukemia stem cell (LSC), which we designate as monocytic LSC (m-LSC), that is developmentally and clinically distinct from the more well-described primitive LSC (p-LSC). The m-LSC is distinguished by a unique immunophenotype (CD34-, CD14-, CD14-, CD36-), unique transcriptional state, reliance on purine metabolism, and selective sensitivity to cladribine. Critically, in some instances, m-LSC and p-LSC subtypes can co-reside in the same patient with AML and simultaneously contribute to overall tumor biology. Thus, our findings demonstrate that LSC heterogeneity has direct clinical significance and highlight the need to distinguish and target m-LSCs as a means to improve clinical outcomes with venetoclax-based regimens.

**SIGNIFICANCE:** These studies identify and characterize a new type of human acute myeloid LSC that is responsible for monocytic disease progression in patients with AML treated with venetoclax-based regimens. Our studies describe the phenotype, molecular properties, and drug sensitivities of this unique LSC subclass.

LSC types.

## INTRODUCTION

Numerous studies have described the properties of malignant stem cells that drive the pathogenesis of myeloid leukemias (1). Analyses of primary human tissue specimens, as well as many different mouse models, have consistently shown that leukemia stem cells (LSC) are biologically distinct from bulk tumor populations and frequently demonstrate drugsensitivity/resistance profiles that differ from the majority of leukemic cell types (2). Analogous to normal hematopoietic stem cells, conventional LSCs are also thought to be mostly quiescent and capable of giving rise to progeny that comprise the overall tumor population. As such, LSCs represent a critical target in the development of novel therapies. Previous attempts to target the LSC population have been

We posit that a major challenge in targeting LSCs lies in the inherent heterogeneity of malignant stem cells (3). As reported by multiple previous studies, LSC populations derived from human AML patients demonstrate significant intra- and interpatient heterogeneity in developmental stages and immunophenotypes (4–9). Furthermore, single-cell studies have begun to describe underlying genetic diversity that may contribute to LSC heterogeneity (10, 11). Thus, to improve clinical outcomes from LSC-targeting therapies, it is likely critical to understand the properties of heterogeneous LSC subtypes and use therapeutic strategies that either target common vulner-

abilities or are designed to simultaneously eradicate differing

made, including focusing on specific cell-surface antigens, metabolic interventions, epigenetic strategies, mutation-tar-

geted approaches, immune-based therapies, and more (2).

Although multiple strategies derive from robust experimen-

tal evidence, improvement of clinical outcomes due to direct

eradication of LSCs has remained limited.

<sup>1</sup>Bone Marrow Transplantation Center, the First Affiliated Hospital, School of Medicine, Zhejiang University, Hangzhou, China. <sup>2</sup>Liangzhu Laboratory, Zhejiang University, Hangzhou, China. <sup>3</sup>Institute of Hematology, Zhejiang University, Hangzhou, China. <sup>4</sup>Zhejiang Province Engineering Laboratory for Stem Cell and Immunity Therapy, Hangzhou, China. <sup>5</sup>Division of Hematology, University of Colorado School of Medicine, Aurora, Colorado. <sup>6</sup>Rocky Mountain Regional VA Medical Center, Aurora, Colorado. <sup>7</sup>University of Colorado Cancer Center, University of Colorado Anschutz Medical Campus, Aurora, Colorado. <sup>8</sup>Department of Immunology and Microbiology, University of Colorado Anschutz Medical Campus, Aurora, Colorado. <sup>9</sup>Center for Cancer and Blood Disorders, Department of Pediatrics, University of Colorado, Aurora, Colorado. <sup>10</sup>Department of Pathology, University of Colorado School of Medicine, Aurora, Colorado.

Note: S. Pei and I.T. Shelton contributed equally to this article.

Corresponding Authors: Craig T. Jordan, Division of Hematology, University of Colorado Anschutz Medical Campus, 12700 East 19th Avenue, Room 9122, RC2, Campus Box B170, Aurora, CO 80045. Phone: 585-747-1388; E-mail: craig.jordan@cuanschutz.edu; and Shanshan Pei, Zhejiang University, Liangzhu Laboratory, Office 518, 1369 Wenyixi Road, Yuhang, Hangzhou, Zhejiang, China. Phone: 86-0571-88790516; E-mail: shanshan.pei@ziu.edu.cn

Cancer Discov 2023;13:■■■-■■■

doi: 10.1158/2159-8290.CD-22-1297

©2023 American Association for Cancer Research

To better elucidate the nature of LSC heterogeneity, we recently described an analysis of patients who relapsed following treatment with the recently FDA-approved regimen containing the BCL2 inhibitor venetoclax in combination with azacitidine (12). These studies demonstrated two key findings. First, we observed that relapsed patients can in some cases develop a transcriptionally and immunophenotypically mature monocytic disease, morphologically categorized as M5 but not M4 by the French-American-British (FAB) system (12, 13). This finding is quite distinct from patients treated with conventional chemotherapy who almost invariably relapse, with disease that shows a more transcriptionally primitive phenotype (12, 14). Second, these studies suggest that stem cells driving monocytic relapse may be biologically distinct from the LSCs that create more primitive de novo disease. Together, these findings indicate the existence of heterogeneous underlying LSC populations that mediate differing therapeutic outcomes of conventional chemotherapy and venetoclax-based therapies. In the present study, we performed an in-depth analysis of

human AML patient specimens as a means to identify and characterize LSC heterogeneity that may drive the evolution of disease in response to venetoclax-based regimens and explored therapeutic regimens that can perturb this evolution, allowing improved treatment outcomes.

## **RESULTS**

# Characterization of Developmentally Heterogeneous LSCs

As a resource for the studies described herein, we first analyzed a cohort of 20 primary human patient specimens that were selected to represent the spectrum of phenotypes commonly encountered in AML (Supplementary Table S1). As illustrated in Fig. 1A, we defined three broad classes of specimens: predominantly primitive (Prim), mixed monocytic-primitive (MMP), and predominantly monocytic (Mono). As indicated by standard flow cytometric blood cell gating, the Prim specimens display almost no differentiated monocytic features (<1%) and a predominant blast-like profile [defined as CD45-medium and low internal side scatter (SSC) relative to lymphocytes from the same patients]. Prim specimens express high levels (>90% in most) of the canonical stem/progenitor-associated markers CD34 or CD117 and low collective levels of monocytic antigens (CD11b, CD64, CD14, CD36, or LILRB4; Supplementary Fig. S1A). In contrast, at the most differentiated end of the myeloid spectrum, Mono specimens display very few blast-like cells (<1%) and a predominant monocyte-like profile in the CD45/SSC gate (CD45-bright, and SSC-high relative to lymphocytes). Mono specimens downregulate CD34 and CD117 and strongly upregulate at least two monocytic markers, particularly CD64 (Supplementary Fig. S1B). Finally, MMP specimens are characterized as having discrete blastlike and monocytic-like subpopulations (range, 26%-79% for primitive and 14%-35% for monocytic), which are evident in both the CD45/SSC gate and phenotypic analysis of stem/progenitor markers and monocytic antigens (Supplementary Fig. S1C).

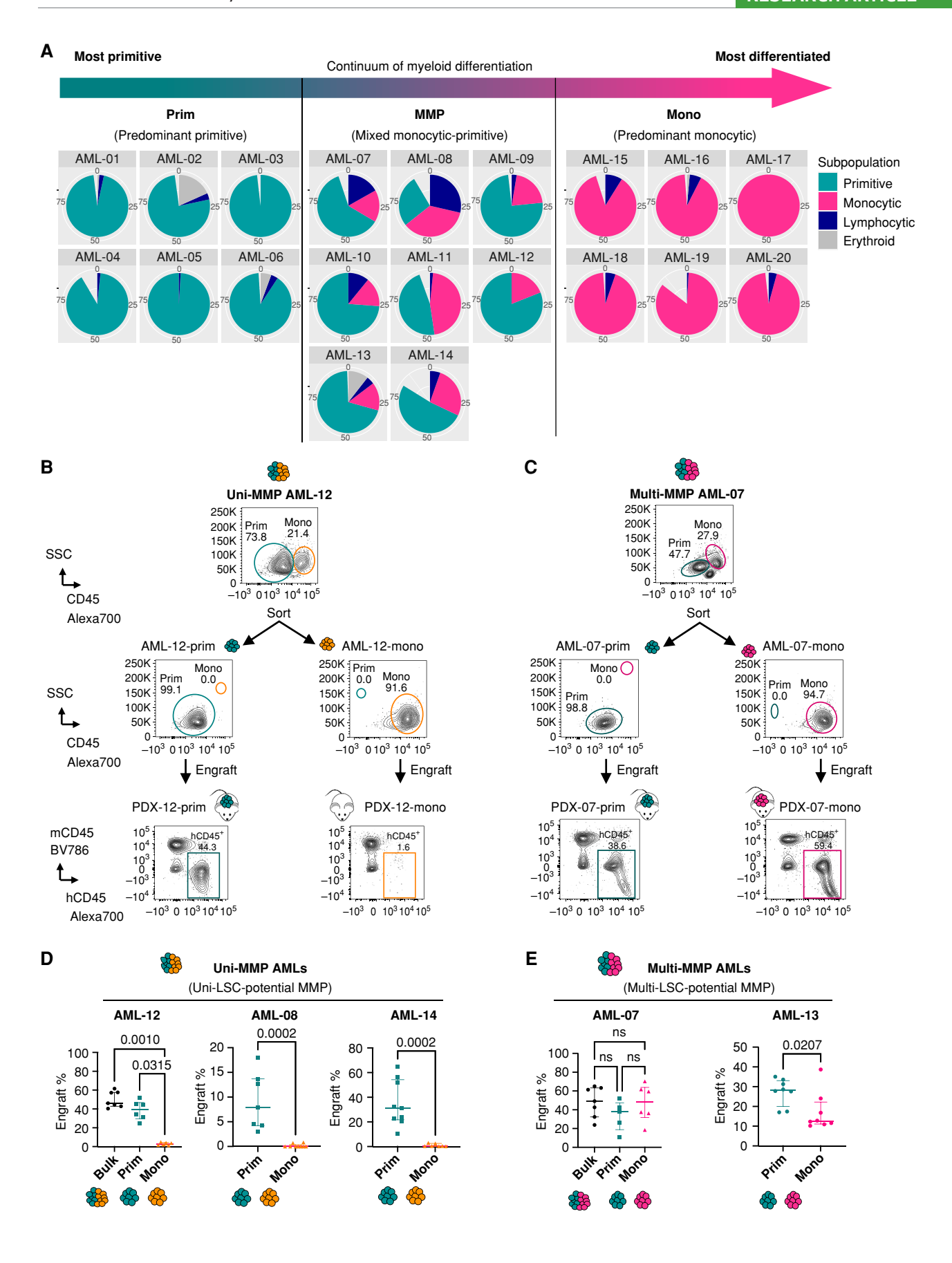
We hypothesized that heterogeneity within the LSC compartment may contribute to the developmental heterogeneity illustrated in Fig. 1A. To begin to characterize potential LSC heterogeneity, we performed flow cytometric cell sorting to isolate primitive (prim) and monocytic (mono) subpopulations from several MMP AMLs. Each subpopulation was independently transplanted into immunodeficient NOD.Cg-*Prkdc*<sup>scid</sup> *Il2rg*<sup>tm1Wjl</sup> Tg(CMV-IL3,CSF2,KITLG)1Eav/MloySzJ (NSG-S) mice and evaluated for engraftment of leukemic disease by measuring the percentage of human CD45<sup>+</sup> cells in the bone marrow of each experimental animal (Fig. 1B and C). These studies revealed two distinct types of MMP AML patients. One we term "Uni-MMP," in which LSC activity was exclusively detected in the prim but not in the mono subpopulation

(Fig. 1D). In contrast, the second type of MMP AML we term "Multi-MMP," in which readily detectable LSC activity was evident in both prim and mono subpopulations (Fig. 1E).

To assess the underlying mutational profile of the Uni- and Multi-MMP types of AML, whole-exome sequencing (WES) was performed on flow-sorted prim and mono subpopulations. As shown in Supplementary Fig. S1D (detailed in Supplementary Table S2), WES analysis indicated that the prim and mono subpopulations from three independent Uni-MMP specimens had a comparable mutational profile in the 49 commonly mutated genes of AML (listed in Supplementary Table S3). A few differences in variant allele frequency were noted (see AML-12 FLT3 and AML-8 SETBP1 mutations), but overall, the analyses were consistent with a common genetic origin. WES of three Multi-MMP specimens showed two with similar profiles between prim and mono subpopulations (AML-07 and AML-13); however, the third specimen (Pt-12; Supplementary Fig. S1D) demonstrated a clear difference, with differing NRAS and SMC1A mutations in the two fractions. Interestingly, Pt-12 showed multiple mutations in common including IDH2 and SRSF2 between the prim and mono subpopulations, suggesting that divergence occurred at a relatively late stage of pathogenesis from a common ancestor clone. These initial data indicate that in at least some instances Multi-MMP AML arises due to underlying mutational variation. These findings corroborate and extend several previous studies demonstrating that phenotypically distinct subpopulations of LSCs can simultaneously exist in certain patients with AML (6-9).

To further characterize the leukemogenic properties of LSCs in Multi-MMP patients, the nature of disease arising in transplanted NSG-S mice was evaluated. As shown in Fig. 2A and Supplementary Fig. S2A and S2B, prim- versus mono-engrafted cells from two representative specimens (AML-07 and AML-13) consistently differed in their developmental spectrum. For both AMLs, the prim subpopulation was able to recapitulate the full developmental spectrum of disease, with both prim and mono cells evident in each transplanted mouse. In contrast, the mono subpopulation only gave rise only to monocytic disease, with no evidence of more primitive cells. Importantly, such distinct differences in the developmental spectrum of engrafted disease can translate into clear differences in therapeutic sensitivity. When prim- versus mono-engrafted groups from AML-07 were treated with a regimen of venetoclax plus azacitidine (VEN + AZA) in vivo (Fig. 2B and C), the mono-derived disease was significantly more resistant to VEN + AZA than the prim cells (Fig. 2D). Thus, the LSCs that initiate and drive disease in the monocytic subpopulation demonstrate a more restricted developmental hierarchy that resides toward the mature end of the myeloid developmental spectrum and distinct resistance to VEN + AZA therapy. We designate this subclass of LSCs as mono-LSCs (m-LSC) in contrast

**Figure 1.** Characterization of developmentally heterogeneous LSCs. **A,** Pie charts showing the relative proportion of cells at primitive (teal), monocytic (pink), lymphocytic (dark blue), and erythroid (gray) stages for each primary AML. **B** and **C,** Sorting strategy and engraftment of prim and mono subpopulations from representative Uni-MMP AML-12 and Multi-MMP AML-07, respectively. The CD45/SSC flow plots in the top row depict leukemia disease before sort. The CD45/SSC flow plots in the middle demonstrate cells after sort. The human-CD45/mouse-CD45 (hCD45/mCD45) flow plots in the bottom row show engraftment levels in bone marrow of representative recipient mice. Percentage of hCD45\*/mCD45\* cells was used to quantify engraftment levels. PDX, patient-derived xenograft. **D** and **E**, Summary of engraftment data for Uni-MMP (AML-12, AML-08, and AML-14) and Multi-MMP (AML-07 and AML-13), respectively. Bulk stands for unsorted bulk tumor; prim stands for primitive subpopulation; and mono stands for monocytic subpopulation. Each dot represents a mouse. AML-12 (bulk, n = 7; prim, n = 6; mono, n = 6). AML-08 (prim, n = 7; mono, n = 9). AML-14 (prim, n = 9; mono, n = 7). AML-07 (bulk, n = 7; prim, n = 6). AML-13 (prim, n = 8; mono, n = 8). Median ± interquartile range. Two-tailed Mann-Whitney tests were used for comparing two groups, and Kruskal-Wallis tests were used when comparing more than two groups. ns, not significant.



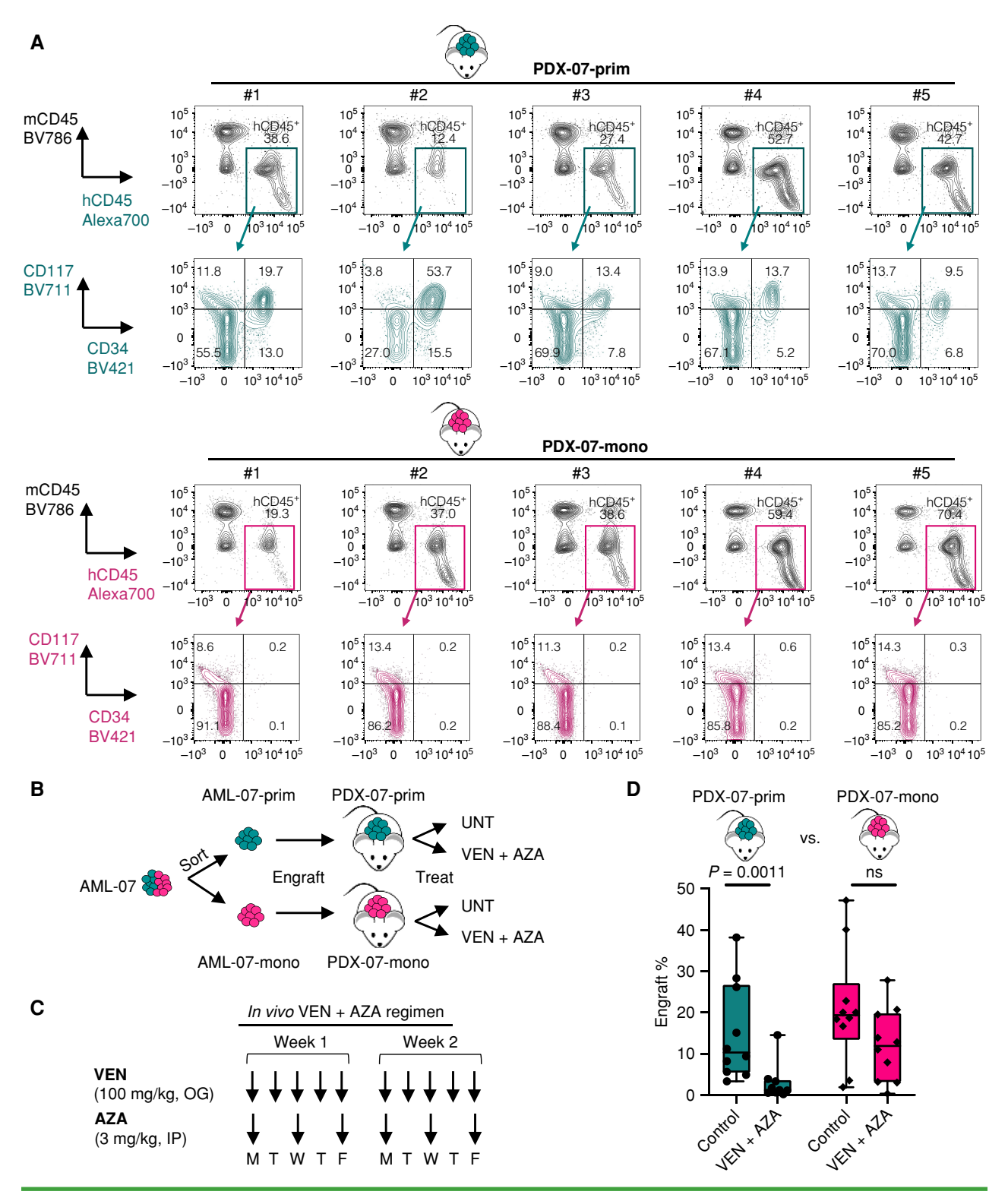


Figure 2. Differing nature of disease arising from prim and mono subpopulations of Multi-MMP AMLs. **A**, Representative flow plots showing immunophenotypic differences between leukemia arising from prim and mono subpopulations of Multi-MMP AML-07 in NSG-S mice. Five representative mice from each group are shown. For each mouse, engrafted human leukemic cells were gated as hCD45\*/mCD45\* (teal and pink gates), and their expression patterns of CD34 and CD117 are shown to illustrate immunophenotypic differences between the two groups. PDX, patient-derived xenograft. **B**, A diagram depicting workflow used to isolate primitive and monocytic subpopulations of AML-07 for injecting into PDX mice and subsequent determination of their relative sensitivity to the VEN + AZA regimen *in vivo*. UNT, untreated. **C**, Design of the VEN + AZA *in vivo* regimen. **D**, Impact of *in vivo* VEN + AZA treatments on leukemia engrafted from prim vs. mono subpopulations of AML-07. Engraft% was determined by % of hCD45\*/mCD45\* cells within total viable bone marrow cells. Each dot represents a unique mouse. PDX-07-prim (control, n = 10; VEN + AZA, n = 10), PDX-07-mono (control, n = 10; VEN + AZA, n = 10). Box plots show median  $\pm$  interquartile range. Two-tailed Mann-Whitney test was used. IP, intraperitoneal; ns, not significant; OG, oral gavage.

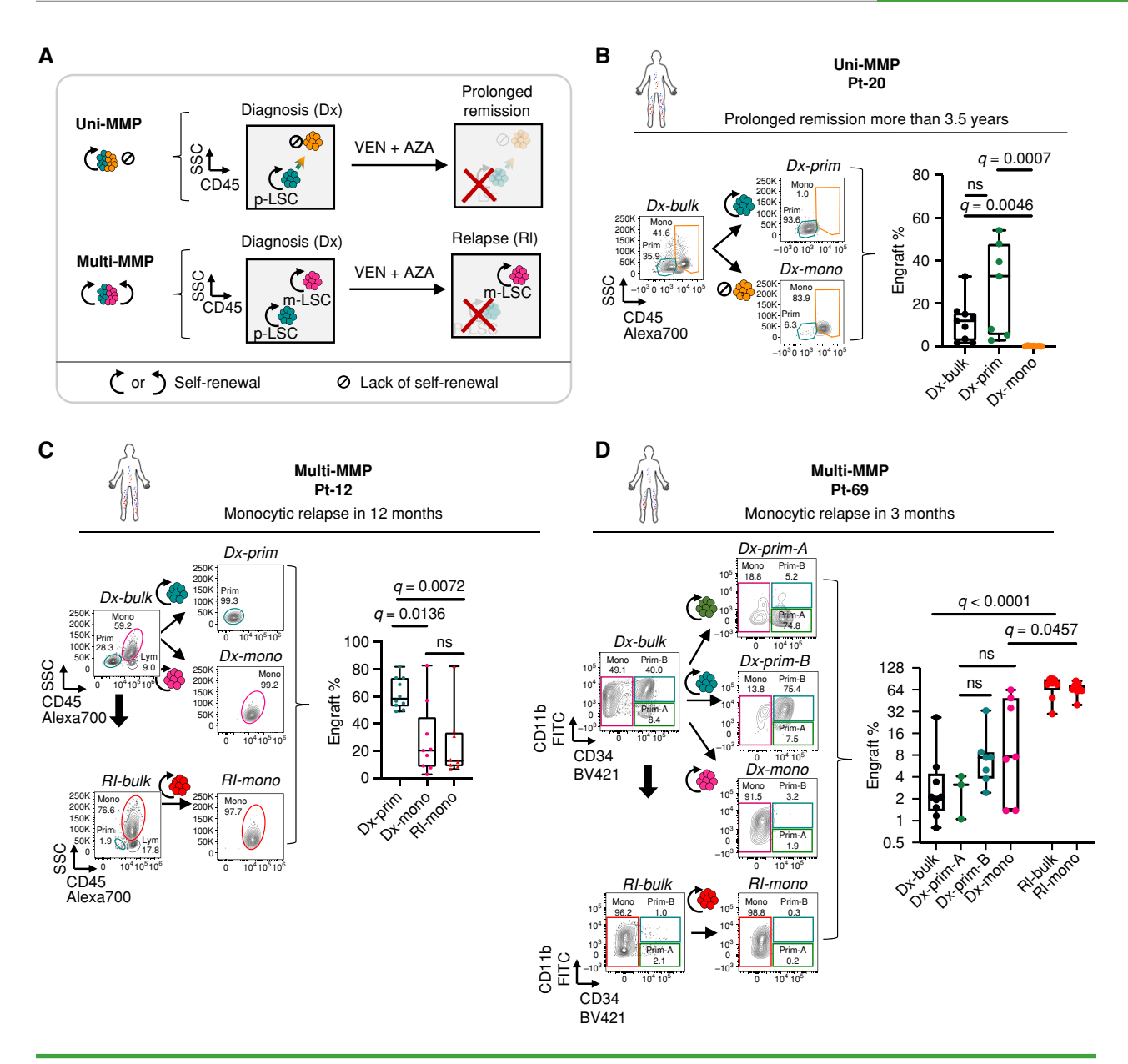
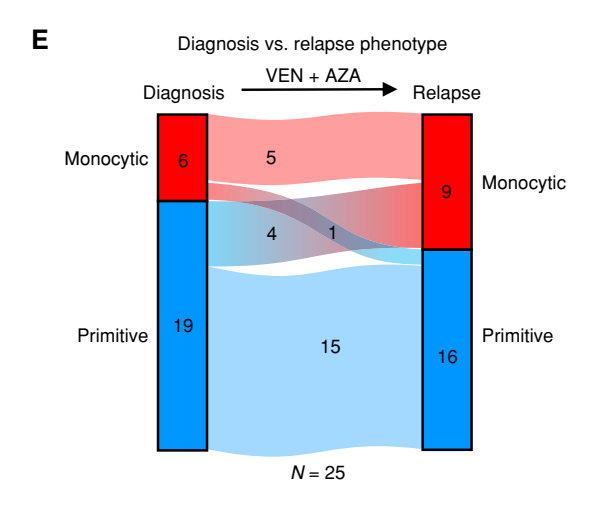


Figure 3. Clinical outcomes as a function of m-LSCs. **A**, A diagram describing the leukemogenesis process of Uni-MMP and Multi-MMP AML patients and their predicted clinical responses to VEN + AZA therapy. **B-D**, Representative cases of Uni-MMP and Multi-MMP AML patients received VEN + AZA therapy. Left, sorting strategies for obtaining diagnosis-prim (Dx-prim) and diagnosis-mono (Dx-mono) subpopulations from diagnosis bulk disease (Dx-bulk), as well as relapse-mono (RI-mono) subpopulations from relapse bulk disease (RI-bulk) when applicable. Right, engraft% in NSG-S mice determined by hCD45+McD45-% within total viable bone marrow cells. Each dot represents a unique mouse. Median  $\pm$  interquartile range. Mann-Whitney tests. ns, not significant. **B**, Patient 20 (Pt-20), a case of Uni-MMP AML presenting prolonged remission after VEN + AZA therapy for more than 3.5 years. Dx-bulk (n = 9), Dx-prim (n = 7), and Dx-mono (n = 7). **C**, Patient 12 (Pt-12), a case of Multi-MMP AML presenting predominant monocytic relapse in 12 months after receiving VEN + AZA therapy. Dx-prim (n = 10), Dx-mono (n = 9), and RI-mono (n = 8). **D**, Patient 69 (Pt-69), a case of Multi-MMP AML presenting quick relapse in 3 months after VEN + AZA therapy. In this particular case, prim and mono subpopulations were gated using a different sorting strategy based on primitive antigen CD34 and monocytic antigen CD11b. For the patient's diagnosis sample, the CD34+/CD11b-, CD34+/CD11b+, and CD34-/CD11b-partially positive (pp) subpopulations were sorted as Dx-prim-A, Dx-prim-B, and Dx-mono subpopulations, respectively. For the patient's relapse sample, the CD34-/CD11b-pp subpopulation was sorted as the predominant RI-mono subpopulation. Dx-bulk (n = 9), Dx-prim-A (n = 3), Dx-prim-B (n = 7), Dx-mono (n = 7), RI-bulk (n = 9), and RI-mono (n = 9). (continued on next page)

to the more conventional prim-LSCs (p-LSC). These findings indicate that heterogeneous LSC subpopulations with distinct developmental phenotypes can co-reside in the same patient. Moreover, LSC heterogeneity gives rise to bulk tumor populations with differing therapeutic response in patient-derived xenograft (PDX) models, implying clinical significance.

#### Clinical Outcomes as a Function of m-LSCs

Based on the above findings and our previous studies (12), we hypothesized that patients with *de novo* AML would differ in pathogenesis and clinical outcome as a function of the presence of m-LSCs. As illustrated schematically in Fig. 3A, we predict that upon receiving VEN + AZA therapy,



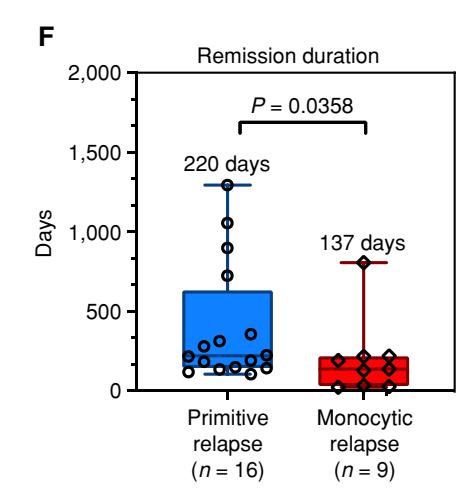


**Figure 3.** (Continued) **E**, Phenotypic changes from diagnosis to relapse in a cohort of patients with AML who received VEN + AZA therapy (N = 25). **F**, Remission duration for AML patients with monocytic relapse (n = 9) vs. primitive relapse (n = 16). Each dot represents a unique patient. Median duration time of both groups is shown in days. In **B-D** and **F**, box plots represent median  $\pm$  interquartile range. In **B-D**, the Kruskal-Wallis test was used. In **F**, the one-tailed Mann-Whitney test was used. ns, not significant.

Uni-MMP patients who initially present with only p-LSCs should achieve more durable remission due to intrinsic reliance of p-LSCs on the venetoclax target, BCL2 (12). In contrast, Multi-MMP patients with a distinct m-LSC population are predicted to relapse relatively quickly with monocytic disease. To test this concept, we evaluated serial specimens obtained from three patients with de novo AML who had been treated with VEN + AZA therapy. As illustrated in Fig. 3B-D, at diagnosis, patient Pt-20 had no detectable m-LSC activity, whereas patients Pt-12 and Pt-69 had readily detectable m-LSC activities as revealed by xenograft assays. Importantly, the presence of functionally defined m-LSCs directly correlated with clinical outcomes, in which Uni-MMP patient Pt-20 experienced prolonged remission for more than 3.5 years (Fig. 3B), and Multi-MMP patients Pt-12 and Pt-69 had a relatively rapid relapse of disease with a monocytic phenotype within 12 and 3 months, respectively (Fig. 3C and D).

To assess mutational changes that may occur during pathogenesis, WES analysis was performed on the sorted prim and mono subpopulations of Pt-20, 12, and 69. As expected for a Uni-MMP AML, Pt-20 showed a very similar mutation profile between prim- and mono-sorted cell populations (Supplementary Fig. S3A and Supplementary Table S2). In contrast, both patients 12 and 69 demonstrated differing mutations. As previously shown in Supplementary Fig. S1D (and shown again in Supplementary Fig. S3A for comparison), Pt-12 had an NRAS mutation specific to the mono subpopulation at diagnosis that remained at relapse. Conversely, Pt-12 had an SMCA1 mutation in the prim subpopulation at diagnosis that was absent at relapse. The data clearly suggest the outgrowth of the genetically defined monocytic subclone. Similarly, Pt-69 had chromosome 11 and 16 duplication events in the prim compartment at diagnosis that were not present at relapse, again consistent with the outgrowth of the genetically distinct monocytic subclone (Supplementary Fig. S3B). Lastly, for comparative purposes, data from Pt-65, which we previously reported (12), are included in Supplementary Fig. S3A. This specimen also shows the outgrowth of genetically distinct monocytic clones at relapse marked by two *KRAS* mutations. Notably, both of the *KRAS* mutations that were dominant at relapse were not readily detectable at 400× sequencing depth in the diagnosis specimen and were seen only using higher resolution methods (droplet-digital PCR). These data suggest even minor monocytic subclones can be selected by the strong selective pressure of VEN + AZA *in vivo* 

To extend our analyses, we subsequently analyzed a cohort of 25 patients with AML who relapsed from VEN + AZA therapy (Supplementary Table S4). We found that nine patients, including five phenotypically monocytic and four who were primitive at diagnosis, relapsed with monocytic features, representing 36% of overall cases (Fig. 3E). Importantly, patients who relapsed with monocytic features also had a significantly shorter remission duration than patients who relapsed with a primitive immunophenotype (Fig. 3F; Supplementary Fig. S3C), suggesting that patients with preexisting m-LSCs may represent an especially poor prognosis subgroup when receiving VEN + AZA therapy. Overall, these findings indicate that the presence of m-LSCs in patients newly diagnosed with AML represents a distinct disease entity and directly predicts the pathogenesis of disease in response to VEN + AZA therapy.

#### Identification of the m-LSC Immunophenotype

Given the unique developmental properties and significant therapeutic impact of m-LSCs, we next sought to identify them in primary AML specimens and begin to characterize their biology. To this end, we used CITE-seq (Cellular Indexing of Transcriptomes and Epitopes by Sequencing) analysis allowing the simultaneous measurement of protein-based surface antigen expression (Supplementary Table S5) and RNA-based transcriptome analysis of primary AML specimens at a single-cell level. We performed CITE-seq analysis on a cohort of 27 primary AML specimens containing immunophenotypically

and functionally defined Prim, Uni-MMP, Multi-MMP, and Mono specimens (listed in Supplementary Table S6). First, we performed clustifyr analysis of the CITE-seq dataset (15, 16), a program that assigns cells to various lymphoid, erythroid, and myeloid cell types according to their similarity to normal hematopoietic counterparts (Supplementary Fig. S4A). These assignments were strongly supported by the expression patterns of classic lineage-specific surface antigens such as CD7, CD56, CD19, CD33, CD34, CD11b, and CD123 (Supplementary Fig. S4B and S4C), as well as lineage-specific transcriptional factors and markers such as GATA2, CEBPA, SPI1/PU.1, AZU1, TCF7, and PAX5 (Supplementary Fig. S4D). We then performed scArches analysis on the myeloid subpopulation to identify cell types that are indicative of the myeloid developmental hierarchy as described in the studies by Zeng and colleagues and Lotfollahi and colleagues (14, 17). This analysis revealed a diverse mixture of cell types (as termed by Zeng colleagues: leukemia stem and progenitor cell (LSPC)-quiescent, LSPCprimed, LSPC-cycling, granulocyte-macrophage progenitor (GMP)-like, promonocyte (ProMono)-like, Mono-like, and conventional dendritic cell (cDC)-like leukemic cells), demonstrating a clear developmental hierarchy from top left to bottom right in the myeloid subpopulation of our primary AML cohort (Fig. 4A). Next, we segregated the overall CITE-seq dataset into Prim, Uni-MMP, Multi-MMP, and Mono groups (Fig. 4B and C). The relative proportions of cell types among the groups were highly concordant with their expected identity. The Prim group almost exclusively contains the three LSPC cell types (quiescent, primed, and cycling), which reside at the apex of the myeloid developmental hierarchy. In contrast, the Mono group presents a developmental hierarchy with almost no LSPC cell types but is rather comprised of a dominant ProMono-like cell type, suggesting the latter could be enriched for m-LSCs. Consistent with this assumption, both LSPC and ProMonolike cell types are present in the Multi-MMP, whereas only the former is present in the Uni-MMP group (Fig. 4B and C).

To further test which cell type might be enriched for LSC activities, we screened several known LSC signatures using our CITE-seq dataset. Interestingly, a KMT2A-rearranged leukemia-specific LSC signature (KMT2A-r\_LSC\_signature; Supplementary Table S7) derived from the studies by Hess and colleagues and Somervaille and colleagues (18-20) matched well with the ProMono-like cell type uniquely present in the Mono and Multi-MMP groups (Fig. 4D). Of note, previous studies have shown that KMT2A-rearranged leukemia is distinct from other AMLs (21), is frequently associated with a monocytic immunophenotype (22), and has LSC characteristics that are distinct from conventional CD34<sup>+</sup> primitive LSCs (23). Consistently, a CD34<sup>+</sup> primitive LSC signature (CD34+\_LSC\_signature, Supplementary Table S7) derived from studies by Eppert and colleagues and Ng and colleagues (24, 25) matched well with LSPCprimed but not ProMono-like clusters in our CITE-seq dataset (Fig. 4D), further supporting the concept that the ProMono-like cell type could be enriched for m-LSC activities. Finally, expression analysis of the surface antigens revealed that the ProMono-like cells are largely CD4+, CD14-, CD11b-, and CD36- relative to other myeloid

leukemia cells, providing a candidate immunophenotype for m-LSCs (Fig. 4E).

#### Functional Validation of m-LSCs

Based on the CITE-seq analysis in Fig. 4, we next performed a series of flow sorting and transplant studies to functionally validate the m-LSC immunophenotype. We initially used two Mono specimens, AML-16 and AML-20, and isolated various subpopulations of cells based on expression of CD45, CD34, CD4, CD14, CD11b, and CD36. To avoid contamination from conventional CD34+ p-LSCs, we gated on the CD34<sup>-</sup> fraction when sorting various subpopulations for measuring m-LSC activities (Fig. 5A and B; Supplementary Fig. S5A and S5B). As shown in Fig. 5C and D and Supplementary Fig. S5C and S5D, functional analysis of each subpopulation demonstrated that the majority of m-LSCs are enriched in the immunophenotype of CD34<sup>-</sup>, CD4<sup>+</sup>, CD14-, CD11b-, and CD36- (designated as D subpopulation). Importantly, transplantation of animals originally engrafted with m-LSC-enriched D subpopulation also demonstrated robust secondary engraftment, indicating strong self-renewal potential. Notably, in AML-20, some engraftment potential was detected in the CD14-, CD11b+, and CD36+ E subpopulation (Fig. 5D), suggesting that in certain patients the developmental hierarchy of m-LSC-driven AMLs can be shallower than others such as AML-16. We also applied a similar approach to validate m-LSCs in Multi-MMP patients. To this end, we used AML-07, which was functionally defined to be a Multi-MMP specimen (Figs. 1 and 2). As shown in Fig. 5E and F and Supplementary Fig. S5E and S5F, serial transplant experiments demonstrated that m-LSCs in this Multi-MMP AML were also exclusively enriched by the CD34<sup>-</sup>, CD14<sup>-</sup>, CD11b<sup>-</sup>, and CD36<sup>-</sup> immunophenotype. Of note, CD4 was not included in this sort due to limited cell numbers. Together, these data reveal an m-LSC immunophenotype that is applicable to both Mono and Multi-MMP AMLs, entirely distinct from profiles previously described for the more conventional primitive LSCs (i.e., CD34+, CD38-, etc.; refs. 4, 24, 25).

To further explore the immunophenotype of m-LSCs, we also used analytical flow cytometry to evaluate the expression of several additional cell-surface antigens associated with stem cell activity. As previously reported by Quek and colleagues (8), both CD117 and CD244 were found to be frequently expressed specifically in CD34<sup>-</sup> AML specimens. As shown in Supplementary Fig. S5G, there was no detectable expression of CD117 in the D subpopulation of any of the seven specimens that underwent functional evaluation for the presence of m-LSCs. Similarly, CD244 was detected only at low levels in two of seven specimens. We also investigated expression of the monocytic marker, CD64, as this antigen was prevalent in our original characterization of monocytic relapse (12). We found that CD64 was strongly expressed in six of seven specimens. Finally, when we evaluated the expression of another important LSC marker, GPR56, in our datasets, we found that mRNA expression of GPR56 is almost absent in monocytic AML at both bulk and single-cell resolution (Supplementary Fig. S5H-S5J). Moreover, flow analysis of GPR56 also showed that its protein expression is high in primitive AML cells as expected but is entirely absent in the m-LSC-enriched D subpopulation (Supplementary Fig. S5K

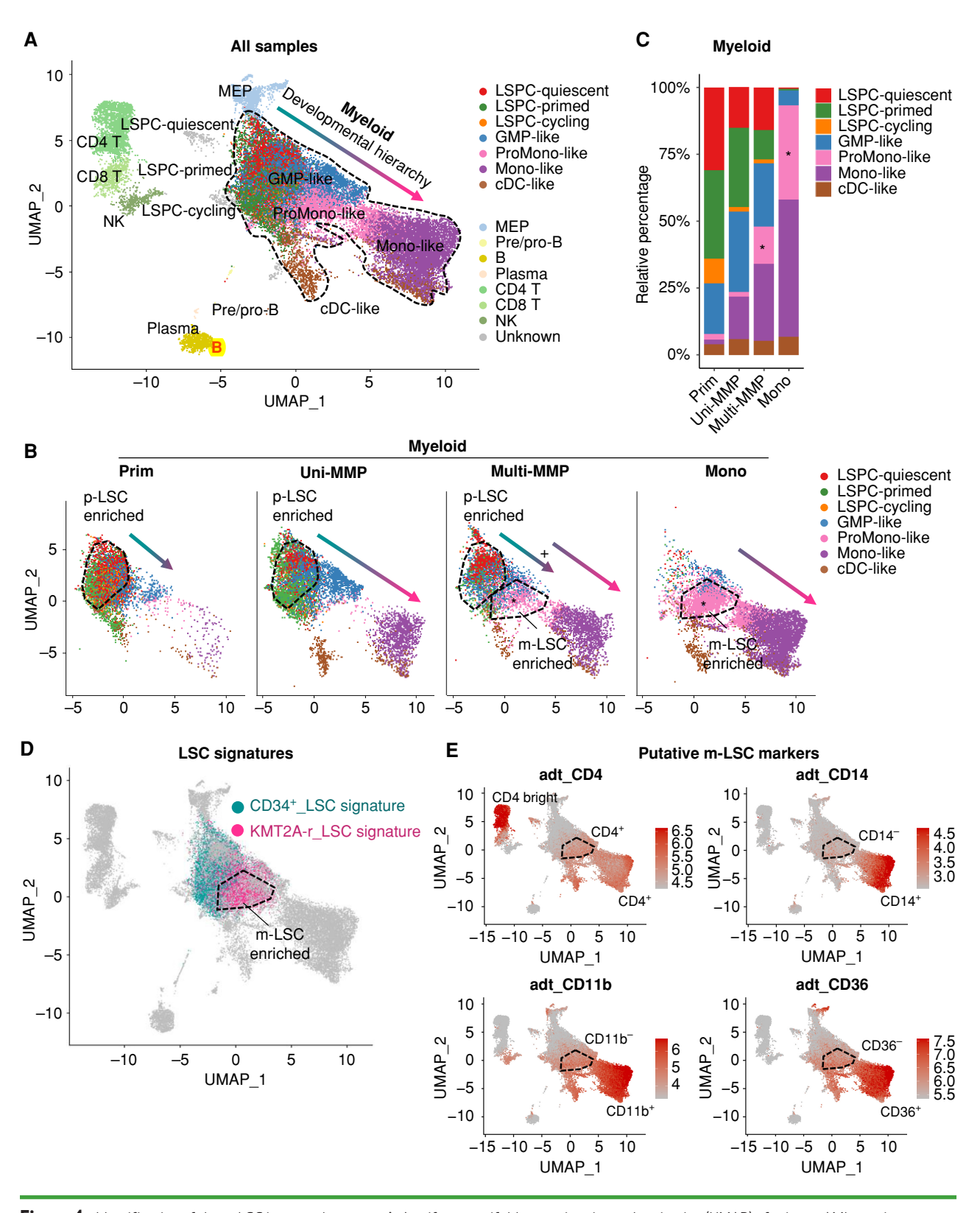


**Figure 4.** Identification of the m-LSC immunophenotype. **A,** A uniform manifold approximation and projection (UMAP) of primary AML specimens (N=27) containing cells of myeloid, lymphoid, and erythroid lineages. Dotted lines highlight the myeloid subpopulation. The colored arrow indicates myeloid developmental hierarchy as revealed by scArches analysis. **B,** UMAPs of immunophenotypically and functionally determined Prim, Uni-MMP, Multi-MMP, and Mono AMLs. Dotted lines highlight areas potentially enriched for p-LSCs and m-LSCs. The colored arrows demonstrate differing developmental hierarchies among the groups. **C,** Stacking bar graphs showing the relative proportion of each subcluster within the myeloid subpopulation. In **B** and **C,** the asterisks mark the cell type that is thought to be enriched for m-LSCs. **D,** Scoring of CD34\*\_LSC and KMT2A-r\_LSC signatures on the UMAP. **E,** Protein expression of surface antigens CD4, CD114, CD11b, and CD36 from CITE-seq analysis.

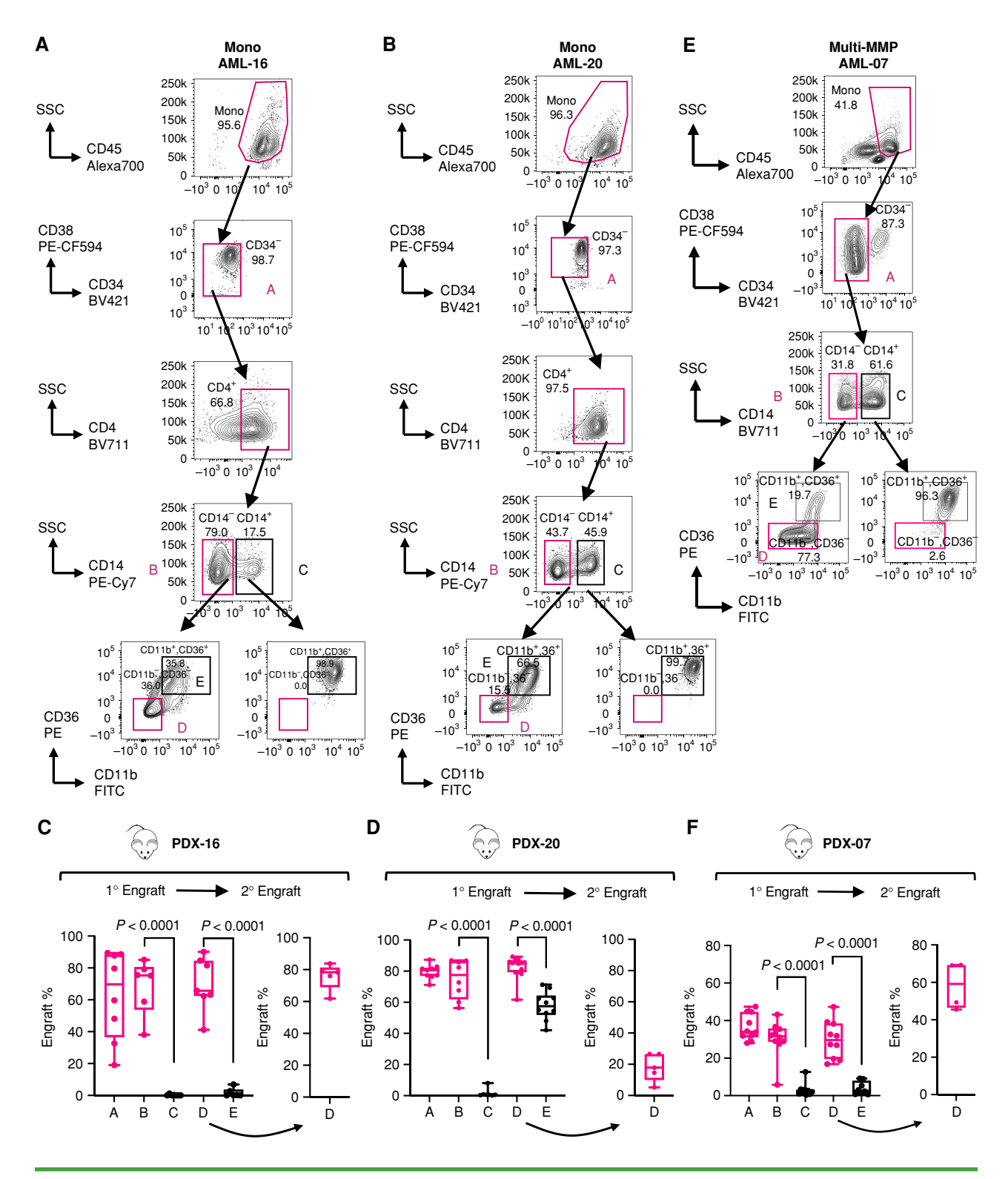


**Figure 5.** Functional validation of m-LSC immunophenotypes. **A** and **B**, Gating strategies for sorting various subpopulations of Mono AML-16 and Mono AML-20 to determine their m-LSC activities using xenograft studies. The sorting is detailed in Supplementary Fig. 5A-C. Briefly, for both specimens, live/mono/CD34-(A), live/mono/CD34-/CD4+/CD14-(B), live/mono/CD34-/CD4+/CD14-(C), (live/mono/CD34-/CD4+/CD14-/CD11b-CD36-(D), and live/mono/CD34-/CD4+/CD14-/CD11b+CD36+(E) were sorted and engrafted. **C** and **D**, Results from transplanting subpopulations of AML-16 [n = 8 (A), n = 6 (B), n = 7 (C), n = 7 (D), n = 6 (E)] and AML-20 [n = 9 (A), n = 8 (B), n = 7 (C), n = 12 (D), n = 10 (E)] are shown as PDX-16 and PDX-20, respectively. **E**, Gating strategies for Multi-MMP AML-07. CD4 was not included in the sort due to the limitation of cells. **F**, Results from transplanting subpopulations of AML-07 [n = 10 (A), n = 10 (B), n = 9 (C), n = 10 (D), n = 8 (E)] are shown as PDX-17. In **C**, **D**, and **F**. Engraft% was determined by % of hCD45-/mCD45-cells within total viable bone marrow cells. Each dot represents a unique mouse. Box plots represent median  $\pm$  interquartile range. Two-tailed Mann-Whitney tests.

and SSL). Thus, although we do not yet have a functional validation of these antigens, we propose that the immunophenotype of m-LSCs will be CD117<sup>-</sup>, CD244<sup>-</sup>, GPR56<sup>-</sup>, and CD64<sup>+</sup>.

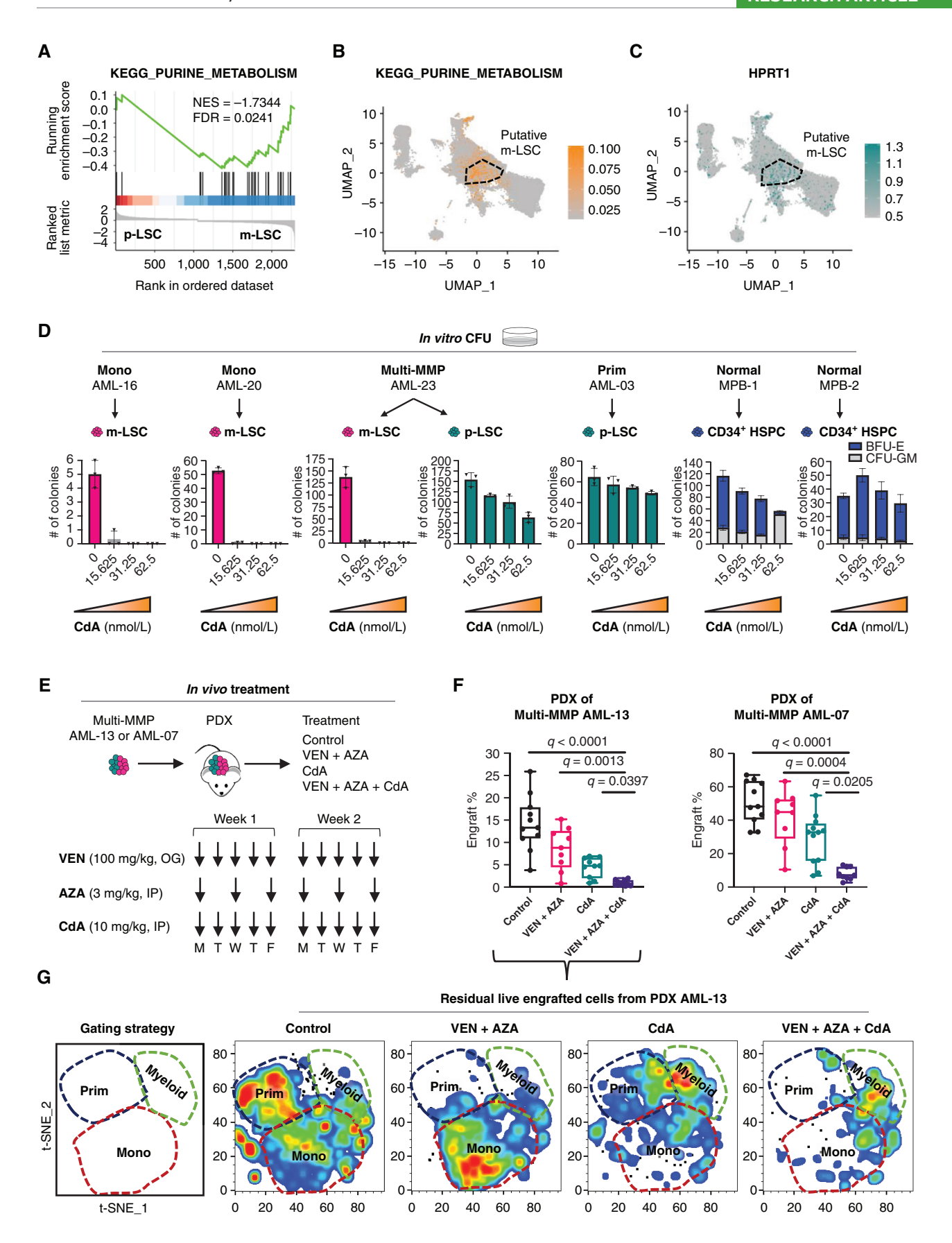
## Targeting Purine Metabolism in m-LSCs

Finally, given the significance of m-LSCs in driving refractory/relapse response to venetoclax-based regimens, we sought to identify potential m-LSC-selective therapies. Using the CITE-seq data described in Fig. 4, we determined that several gene expression signatures were evident in the m-LSC compartment, including purine and pyrimidine metabolism (Fig. 6A and B; Supplementary Fig. S6A and S6B). These results were corroborated by expression patterns of key enzymes known to modulate one-carbon metabolism (e.g., TYMS and DHFR) that feed into purine synthesis (e.g., HPRT1; Fig. 6C; Supplementary Fig. S6C). Consistent with gene expression analyses, metabolic analysis also revealed purine metabolism was enriched in flow-sorted m-LSCs relative to non m-LSCs (Supplementary Fig. S6D and Supplementary Table S8). Hence, we performed functional studies to evaluate agents known to affect these pathways. Specifically, we chose methotrexate (MTX), brequinar (BRQ), and cladribine (CdA), based on previous reports of their respective activities in inhibiting the one-carbon metabolism enzymes DHFR and TYMS (26), pyrimidine synthesis (27), and purine-based DNA/RNA synthesis (28). Colony-forming unit assays were performed on m-LSCs and p-LSCs isolated from Mono, Multi-MMP, and Prim specimens, along with normal CD34+ hematopoietic stem and progenitor cells (HSPC) from two healthy donors. As shown in Fig. 6D and Supplementary Fig. S6E, CdA showed remarkable specificity against m-LSCs while sparing p-LSCs as well as normal HSPC controls. This selectivity was not seen by the other chemotherapy agents cytarabine and daunorubicin (Supplementary Fig. S6F), suggesting the unique sensitivity of m-LSCs to CdA. In addition, CdA also outperformed BRQ and MTX in potency against m-LSCs (Supplementary Fig. S6G). Thus, given its superior selectivity and extensive clinical use (28), CdA was selected for in vivo proof-ofconcept studies in combination with VEN + AZA in two functionally validated MMP AMLs. As shown in Fig. 6E, Multi-MMP AML-13 and AML-07 were transplanted into NSG-S mice and treated with VEN + AZA alone, CdA alone, or the triple-drug combination in vivo. Analysis of AML cells in both bone marrow and spleen demonstrated that the addition of CdA clearly improved the clearance of tumor that was otherwise resistant to VEN + AZA in both PDX models (Fig. 6F; Supplementary Fig. S6H-S6K). Notably, flow analysis of residual engrafted human cells after treatment revealed that the VEN + AZA regimen selectively cleared the primitive subpopulation, whereas the CdA regimen targeted the monocytic counterpart, and the triple-drug regimen eradicated both (Fig. 6G).

## DISCUSSION

The findings presented in this report describe the identification and characterization of a previously unrecognized type of human AML stem cell that we term m-LSC. This particular subclass of LSC is distinguished from more primitive subtypes by virtue of a unique immunophenotype (CD34-, CD4+, CD14-, CD11b-, and CD36-), a relatively narrow developmental hierarchy that is limited to the creation of monocytic progeny, and a gene expression profile that is roughly analogous to normal human promonocytes (ProMono-like). Notably, the m-LSC is distinct from the CD34<sup>-</sup> LSC populations described previously by Quek and colleagues, in which expression of both CD117 and CD244 was prevalent (8). The m-LSC is also different from GPR56+ LSCs described by Pabst and colleagues and Waclawiczek and colleagues (29, 30). The molecular biology of m-LSCs differs from more primitive LSCs in that BCL2 dependency seems to be largely dispensable, making this type of LSC resistant to treatment with venetoclax and azacitidine (31). Further, m-LSCs demonstrate selective reliance on one-carbon metabolism and purine/ pyrimidine metabolism, adding to the importance of cellular metabolism in the context of AML pathogenesis and therapeutic resistance (32-36). Importantly, reliance on purine metabolism appears to mediate increased sensitivity to agents such as CdA, a purine analogue widely used in hematologic malignancies (28). We demonstrate that the addition of CdA to the VEN + AZA regimen increases eradication of primary AML containing m-LSC activity in both in vitro and in vivo preclinical models. We believe these findings provide important mechanistic insights that may explain results from several recent clinical trials reporting superior complete remission (CR)/CR with incomplete hematologic recovery and minimal residual disease negativity rates when venetoclax is combined with chemotherapy regimens, especially ones that contain CdA or its close analogue fludarabine, namely, FLAG-Ida (fludarabine, cytarabine, idarubicin, and G-CSF), CLIA (CdA, idarubicin, and cytarabine), or Clad-LDAC/AZA (CdA plus low-dose cytarabine alternating with azacitidine; refs. 37-40). Notably, the addition of CdA in the above trials seemed to be based on empirical clinical experience and the long history of using CdA-containing chemotherapy regimens for relapse/ refractory stages of AML. Our discovery of m-LSCs and their unique resistance to venetoclax and sensitivity to CdA suggests that the efficacy of these CdA/fludarabine-containing

**Figure 6.** Molecular properties and targeting of m-LSCs. **A**, A gene set enrichment analysis enrichment plot showing upregulation of the purine metabolism pathway in m-LSCs relative to p-LSCs. KEGG, Kyoto Encyclopedia of Genes and Genomes; NES, normalized enrichment score. **B** and **C**, Scoring of the purine metabolism pathway and expression of HPRT1 on uniform manifold approximation and projection (UMAP). **D**, Impact of CdA on colony-forming unit (CFU) potential of m-LSCs, p-LSCs, and CD34+ HSPCs sorted from Mono (AML-16, AML-20), Multi-MMP (AML-23), Prim (AML-03) and two normal mobilized peripheral blood samples (MPB-1, 2). BFU-E, burst-forming unit-erythroid; CFU-GM, colony-forming unit-granulocyte-macrophage. **E**, A diagram depicting workflow and design of the regimens used for *in vivo* treatment. IP, intraperitoneal; OG, oral gavage. **F**, Impact of *in vivo* VEN + AZA, CdA, or triple-drug combo treatments on the bone marrow tumor burden of PDX. Engraft% was determined by % of hCD45+/mCD45- cells within total viable bone marrow mononuclear cells. Each dot represents a unique mouse. For PDX of AML-13, control (*n* = 11), VEN + AZA (*n* = 9), CdA (*n* = 10). For PDX of AML-07, control (*n* = 11), VEN + AZA (*n* = 9). Box plots represent median ± interquartile range. Kruskal-Wallis test was used. ns, not significant. **G**, T-distributed stochastic neighbor embedding (t-SNE) analysis of immunophenotypic data of residual live engrafted cells from PDX of AML-13 after treatment.



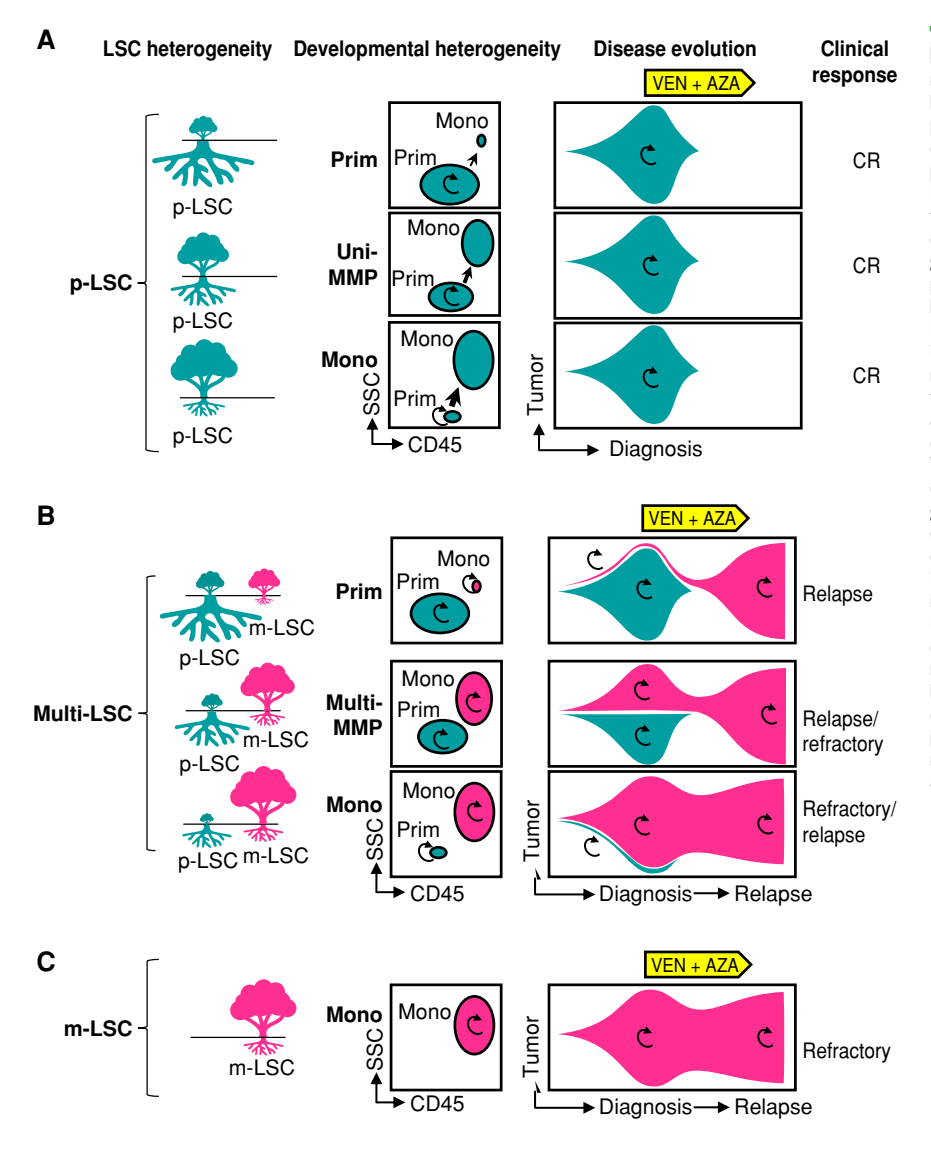


Figure 7. A model depicting m-LSC-driven relapse/refractory responses to venetoclaxbased therapy. A, A first group of AML patients with disease solely driven by p-LSCs captured at various maturation stages with predominant Prim, MMP, and predominant Mono immunophenotypes. The majority of these p-LSCs are expected to be BCL2dependent, rendering a high CR rate in this group of patients. B, A second group of AML patients with multi-LSC activities (contains both p-LSCs and m-LSCs) presenting Prim, MMP, or Mono immunophenotypes depending on the relative degrees of maturation and ratio of the two diseases rooted from the two distinct LSC subtypes. These patients are expected to have a higher tendency to develop relapse/refractory responses to VEN + AZA due to the nature of m-LSCs described in the current study. C. A last group of AML patients with disease solely driven by m-LSCs usually presents a predominant mono immunophenotype due to the inherent nature of m-LSCs that are already resting at a relatively more mature promyelocyte-like developmental stage. This group of patients has a high tendency to develop a refractory response to VEN + AZA, as shown by our previous studies. In all graphs, tealcolored symbols represent p-LSCs and their progenies, pink-colored symbols represent m-LSCs and their progenies, and circular arrows represent self-renewal capacity.

venetoclax regimens may be at least in part due to more comprehensive eradication of the multiple LSC subtypes.

The collective findings from our work suggest the stratification of patients with primary AML based on the nature of underlying LSC heterogeneity. As shown in Fig. 7, we use the tree as an analogy to describe the developmental hierarchy of AML, in which the underground roots represent LSCs and the branches above the ground symbolize more differentiated blasts. In Fig. 7A, a single class of more primitive LSCs (p-LSC) may be present in patients newly diagnosed with AML, with varying degrees of monocytic differentiation potential. In this scenario, no m-LSCs are present, and venetoclax-based therapy would be predicted to confer relatively high CR rates and longer remissions. In contrast, as shown in Fig. 7B, some patients with AML present with at least two distinct subtypes of LSC with primitive versus monocytic characteristics (p-LSC and m-LSC). Depending on the size of the m-LSC population, these patients would be expected to experience brief responses followed by relapse or to be refractory to venetoclax-based therapies. Finally, in more extreme cases, m-LSCs are the dominant population (Fig. 7C), which would likely result in disease that is up-front refractory to venetoclax. Notably, this is exactly what we previously reported; as shown in Supplementary Fig. S7A and S7B, patients who present with the most differentiated monocytic phenotypes (i.e., FAB-M5) but not those with myelomonocytic phenotypes (i.e., FAB-M4) show the highest frequency of refractory disease (12, 13). Moreover, as shown in Fig. 3F, patients relapsed with a monocytic disease have a significantly shorter duration of remission compared with ones that had primitive relapse.

The model described in Fig. 7 has specific ramifications for the design of future therapies. Detection of any m-LSC population at diagnosis in a patient who is being considered for a venetoclax-based therapy may warrant consideration of additional therapies designed to selectively target the monocytic population in the hopes that relapse, which carries a very poor prognosis in this setting (41, 42), can be avoided. Aside from CdA, such potential agents include immunotherapies directed toward monocytic antigens, such as CD64 and LILRB4, or small molecules that selectively impair the unique biology of phenotypically monocytic AML. For example, as we and others have previously reported, MCL1 inhibitor drugs appear

to be more active in the context of monocytic AML (12, 43). Our data suggest this is at least partly due to dependence on MCL1 for energy metabolism in m-LSCs (12). Alternatively, for patients with BCL2-dependent p-LSC disease at diagnosis, no additional therapy beyond venetoclax and azacitidine may be appropriate to allow for durable remissions. For patient whose disease is solely driven by BCL2-independent m-LSCs, one could consider the replacement of venetoclax with another therapeutic strategy more likely to be effective. Future clinical trials designed in this way may serve to optimize outcomes and prevent overtreatment.

Importantly, m-LSC-driven disease propagation and/or relapse is observed only in approximately 30% of patients with AML. However, the emergence of drug-resistant disease eventually occurs in the majority of newly diagnosed patients treated with the VEN + AZA regimen. This finding strongly implies that other subclasses of LSCs are present (or can evolve) in patients treated with venetoclax-based regimens. A recent study by Waclawiczek and colleagues revealed that both BCL2-dependent and BCL2-independent GPR56+ primitive LSCs may exist in patients with primary AML (30), providing a potential explanation for nonmonocytic refractory/ relapse responses following venetoclax-based therapies. Thus, defining additional phenotypes associated with venetoclax-resistant LSCs remains a high priority.

Finally, our study serves to further elaborate the connection between oncogenic mutations, LSC heterogeneity, developmental state of AML, and varying therapeutic responses in the clinic. Our WES analysis showed that mutational profiles can be similar and dissimilar between the prim and mono subpopulations of Multi-MMP patients, suggesting both genetic and epigenetic factors could be contributing to coexisting LSC subtypes within the same patient. We postulate that although different mutational combinations can drive LSC heterogeneity, it is also possible that the same mutations occurring in different cells of origin could be a source for LSC heterogeneity, as evidenced by previous studies in KMT2A-rearranged leukemia (44, 45). Previous studies have established several key elements of this broader picture. First, a recent single-cell multiomic study by Miles and colleagues has drawn strong ties between mutational profiles and immunophenotypes of AML (10). The study found that venetoclax-sensitive IDH mutants tend to express the primitive marker CD34 and conversely venetoclax-resistant RAS mutants usually express monocytic antigen CD11b (10, 46). Second, deconvolution analysis of bulk RNA sequencing data from approximately 1,000 patients with primary AML by Zeng and colleagues has demonstrated a similarly strong association between genotype, phenotype, and drug response at bulk level (14). Of note, a link between RAS mutations and mature monocytic differentiation was particularly strong in this study (14). Third, a recent human study by Zeisig and colleagues showed that LSC activities exclusively exist in the CD34<sup>-</sup> but not the conventional CD34<sup>+</sup> subfraction of KMT2A-rearranged primary AML displaying either CD34<sup>-</sup>/ CD34-low or CD34<sup>+</sup> immunophenotypes (45). Lastly, our previous study suggests that RAS-driven monocytic subclones can be a major driver of monocytic relapse in patients with AML treated with VEN + AZA. The current study reveals a novel type of venetoclax-resistant m-LSC found in both RAS-mutant mono (AML-20), KMT2A-rearranged mono (AML-16), and

Multi-MMP (AML-07, AML-13) contexts (Fig. 5). Thus, taken together, these lines of investigation suggest that complex oncogenic mutations likely converge on limited LSC subtypes that can shape the developmental hierarchy of bulk disease and ultimately affect therapeutic response in the clinic. This model implies that understanding LSC heterogeneity is at the core of improving therapeutic interventions for AML. Besides AML, stem cell architecture can also affect disease progression and predict venetoclax response in myelodysplastic syndrome (47), suggesting malignant stem cell heterogeneity has important ramifications even in early stages of myeloid pathogenesis. Thus, in summary, we postulate that the development of the next generation of precision medicine for AML requires careful dissection of human LSC heterogeneity and discovery of targeted therapies tailored to varying LSC subtypes.

#### **METHODS**

## Primary AML and Normal Mobilized Peripheral Blood Samples

Primary human AML specimens were obtained from leukapheresis product, peripheral blood, or bone marrow of patients with AML who gave written informed consent for sample procurement on the University of Colorado tissue procurement protocols (Colorado Multiple Institutional Review Board Protocol; #12-0173 and #06-0720). All specimens were acquired in accordance with recognized ethical guidelines (Declaration of Helsinki and U.S. Common Rule). Normal mobilized peripheral blood (MPB) specimens were obtained from volunteer donors at the University of Colorado. Age, sex, cytogenetics, and mutation information of primary AML specimens used in the current study are detailed in Supplementary Table S1.

#### Patients, Treatment, and Responses

Twenty-five patients with newly diagnosed AML who received VEN + AZA therapy and had experienced relapse response were included in this study. The patients were diagnosed, treated, and monitored for relapse response over a period from January 2015 to February 2020. The University of Colorado Institutional Review Board approved a request to retrospectively analyze these patients (#19-0115). Diagnosis and relapse phenotypes were determined through morphologic review by hematologists and examination of clinical flow notes when available. Remission duration was calculated as the numbers of days in between the date of best response and the date of relapse. Cytogenetic, mutational information of diagnosis and relapse stages as well as remission duration time are detailed in Supplementary Table S4.

## Processing and Culturing of Primary AML and Normal CD34 $^{\circ}$ HSPCs

Primary human AML specimens and normal MPB samples were resuspended at about 100 to 200 e<sup>6</sup> cells per mL in freezing media composed of 50% FBS (GE HealthCare), 10% DMSO (Sigma), and 40% IMDM (Gibco) and then cryopreserved in liquid nitrogen. Cells were thawed in 37°C water bath and washed twice in thawing media composed of IMDM (Gibco), 2.5% FBS (GE HealthCare), and 10 µg/mL DNase (Sigma). Normal CD34\* HSPCs were enriched from thawed MPB samples using the CD34 MicroBead Kit (Miltenyi Biotec). Cells were cultured in complete serum-free media (SFM) in a 37°C, 5% CO<sub>2</sub> incubator. SFM is composed of IMDM (Gibco), 20% BIT 9500 (STEMCELL Technologies), 10 µg/mL low-density lipoprotein (Millipore), 55 µmol/L 2-Mercaptoethanol (Gibco), and 1% penicillin/streptomycin (Gibco). Complete SFM were made by supplementing the SFM with FLT3, IL3, and SCF cytokines (PeproTech), each at 10 ng/mL.

#### Colony-Forming Assays

Freshly sorted m-LSCs and p-LSCs from primary AMLs or CD34<sup>+</sup> HSPCs isolated from normal mobilized peripheral samples were plated in human methylcellulose (R&D Systems) at about 100,000 to 300,000/mL and 2,000/mL, respectively. Small-molecule inhibitors were directly added to the methylcellulose at the desired final concentration at plating. Colonies were counted 2 to 3 weeks after initial plating.

#### Immunophenotyping of Primary AML

About 0.5 to 1e6 freshly thawed primary AML cells were stained with an immunophenotyping panel containing antibodies against human CD45 (BD Biosciences; cat. #560566, RRID:AB\_1645452), CD34 (BD Biosciences; cat. #562577, RRID:AB\_2687922), CD117 (BD Biosciences; cat. #657871, RRID:AB\_2870438), CD11b (BD Biosciences; cat. #562793, RRID:AB\_2737798), CD64 (BD Biosciences; cat. #563459, RRID:AB\_2738220), CD14 (BD Biosciences; cat. #557742, RRID:AB\_396848), CD4 (BD Bio-sciences; cat. #563033, RRID:AB\_2737965), LILRB4 (BioLegend; cat. #333010, RRID:AB\_ 2234677), CD36 (BD Biosciences; cat. #555455, RRID:AB\_395848), or CD38 (BD Biosciences; cat. #562288, RRID:AB\_11153122) at 4°C for 15 minutes, washed with ice-cold FACS buffer, and resuspended in FACS buffer and analyzed on a BD FACSCelesta flow cytometer (BD). For additional analyses, markers including GPR56 (BD Biosciences; cat. #567212, RRID:AB\_2916507), CD244 (BD Biosciences; cat. #562350, RRID:AB\_11153502), and CD68 (BD Biosciences; cat. #564944, RRID:AB\_2739021) were substituted into the backbone panel above. FCS files were analyzed on FlowJo 10.5.3 (FlowJo, RRID:SCR\_008520). High-dimensional data analysis using dimensionality reduction and automated clustering of concatenated samples was performed in FlowJo using its native platform for running t-distributed stochastic neighbor embedding. A complete list of flow antibodies is in Supplementary Table S5.

## Flow Sorting of Prim and Mono Subpopulations for Xenograft Studies

Freshly thawed primary AML cells were stained with viability dyes and antibodies against human CD45 or CD34 and CD11b. For all specimens except for Pt-69, the prim subpopulation was sorted as CD45-medium, SSC-medium, although the mono subpopulation was sorted as CD45-bright, SSC-medium/high as described previously (12). For Pt-69, prim and mono subpopulations were not readily separable using the CD45/SSC gating strategy. An alternative CD34/CD11b gating strategy was used. From the CD34/CD11b gate, two prim subpopulations were revealed from the diagnosis (Dx) specimen: one as Dx-prim-A displaying a CD34+/CD11b- phenotype and one as Dx-prim-B bearing a CD34+/CD11b+ phenotype. One mono subpopulation was also revealed from the diagnosis (Dx) specimen, named Dx-mono, exhibiting a CD34-/CD11b-partial positive (PP) phenotype. In contrast, at relapse (Rl), a single mono subpopulation showing a CD34<sup>-</sup>/CD11b-PP phenotype was revealed as Rl-mono. All subpopulations were sorted and used for xenograft studies.

### Xenograft Studies

NSG-S mice (RRID:IMSR\_JAX:013062) were used for xenograft studies in this study as previously described (48). Male or female mice ranging in age from 6 to 8 weeks were started on the experiment. Littermates of the same sex were randomly assigned to experimental groups. NSG-S mice were preconditioned 24 hours prior to transplant with 30 mg/kg busulfan (Alfa Aesar) via intraperitoneal injection. The busulfan stock was made fresh at 25 mg/mL in 100% DMSO, and then the stock was diluted 1:10 in prewarmed saline (0.9% NaCl) down to 2.5 mg/mL right before use. The diluted busulfan solution was kept in a 37°C water bath before

intraperitoneal injection to prevent precipitation of busulfan due to low solubility. For comparing the engraftment potential of different subpopulations of a primary AML, each subpopulation was sorted according to its percentage of total viable cells (detailed in Supplementary Table S9). When the cell dose was less than 0.5e<sup>6</sup>/ mouse, mononuclear cells isolated from bone marrow and spleens of naive NSG-S mice were used as carrier cells. The sorted cells with or without the addition of carrier cells were then washed, pelleted. and resuspended in the saline buffer to allow tail-vein injection into NSG-S mice at 0.1 mL per mouse. Fifteen minutes prior to injection, in vivo antihuman CD3 antibody (BioCell; cat. #BE0001-2, RRID AB\_1107632) was added at a final concentration of 1 μg/e<sup>6</sup> cells to prevent potential graft-versus-host disease. During all experiments, the weight of mice was approximately 20 to 30 g, with no animals losing greater than 10% body weight. The mice were kept in ventilated cages and given in vivo treatments when needed in the vivarium at the University of Colorado. The majority of the experiments lasted 6 to 12 weeks. At the end of the experiments, mice were euthanized using carbon dioxide. Bone marrow and spleen were harvested and subjected to red blood cell lysis, and the mononuclear cells were stained with human CD45, mouse CD45 antibodies (BD Biosciences; cat. #564225, RRID:AB\_2716861), and DAPI to determine the percentage of engraftment within viable cells. All animal studies were approved by the University of Colorado Institutional Animal Care and Use Committee (protocol number 00308).

#### In Vivo Treatments

About 2 to 4 weeks after initial transplant, tumor burden in the bone marrow was determined to be above 5% in sentinel mice. Mice were then treated with various *in vivo* regimens as follows. Venetoclax was given at 100 mg/kg via oral gavage, 5 days/week for 2 weeks; azacitidine was given at 3 mg/kg via intraperitoneal injection, 3 days/week for 2 weeks; and CdA was given at 10 mg/kg via intraperitoneal injection, 3 days/week for 2 weeks. All treatments were given in the same 2-week time window when stated together.

## CITE-seq Sample Preparation and Library Construction

Mononuclear cell suspensions were prepared from freshly thawed primary AML specimens cryopreserved in liquid nitrogen. For each specimen, about 1 to 2e6 mononuclear cell suspension was stained with a panel of TotalSeq B antibodies (1 µg/each, BioLegend) and fluorochrome-conjugated flow antibodies for CD45, CD235a (BD Biosciences; cat. #559943, RRID:AB\_397386), and DAPI. Cells were stained in staining buffer (PBS + 2% FBS) for 20 minutes at 4°C. Viable and red blood cell-excluded cells were obtained through sorting DAPI<sup>-</sup>/CD235a<sup>-</sup> cells on a BD Biosciences ARIA II cell sorter. After sorting, cells were washed twice using staining buffer and resuspended to 1,000 cells/ $\mu L$  in PBS with 2% FBS and used immediately for capture. Following cell collection and counting, cells were processed with the 10x Genomics 3' dual index v3.1 library kit with feature barcoding technology for cell-surface proteins. Briefly, 10,000 cells were targeted from the stock suspension of 1,000 cells/ $\mu L$ . Cells were processed following the protocol to generate 3' gene expression libraries as well as Feature Barcode cell-surface libraries. Both libraries were dual-indexed, and samples were quantified by Qubit (Life Technologies) and assessed for size and quality by Tapestation (Agilent). Libraries were normalized and pooled for sequencing on a Novaseq 6000 (Illumina) for paired-end 2 × 150 bp sequencing. Targeted read depth for gene expression libraries was 100,000 reads/ cell or ~500 million paired-end reads/library. Targeted read depth for cell-surface libraries was 40,000 reads/cell or 200 million paired-end reads/library. The panel of CITE-seq antibodies is detailed in Supplementary Table S5.

#### CITE-seq Data Preprocessing

Raw sequencing data for gene expression, antibody-derived tag (ADT; surface protein), and hashing libraries were processed using STARsolo 2.7.8a (ref. 49; STARsolo, RRID:SCR\_021542; https:// github.com/alexdobin/STAR/blob/master/docs/STARsolo.md) with the 10x Genomics GRCh38/GENCODE v32 genome and transcriptome reference (version GRCh38\_2020A; https://support. 10xgenomics.com/single-cell-gene-expression/software/release-notes/ build#GRCh38\_2020A) or a TotalSeq barcode reference, as appropriate. Hashed samples were demultiplexed using GMM-Demux (ref. 50; https://github.com/CHPGenetics/GMM-Demux). Next, cellcontaining droplets were identified using dropkick 1.2.6 (ref. 51; https://github.com/KenLauLab/dropkick) using manual thresholds when automatic thresholding failed, ambient RNA was removed using DecontX 1.12 (ref. 52; https://github.com/campbio/celda), and cells estimated to contain >50% ambient RNA were removed, and doublets were identified using DoubletFinder 2.0.3 (ref. 53; DoubletFinder, RRID:SCR\_018771; https://github.com/chrismcginnis-ucsf/DoubletFinder) and removed. The remaining cells were then filtered to retain only those with >200 genes, 500 to 80,000 unique molecular identifiers (UMI), <10% to 20% of UMIs from genes encoded by the mitochondrial genome (sample dependent based on UMI distributions), <5% of UMIs derived from hemoglobin subunit beta, <20,000 UMIs from ADTs, and >100 to 2,750 UMIs from ADTs (sample dependent based on UMI distribution). Filtered cells were modeled in latent space using TotalVI 0.18.0 (ref. 54; https://github.com/scverse/scvi-tools) to create a joint embedding derived from both RNA and ADT expression data, and corrected for batch effects, mitochondrial proportion, and cell cycle. Scanpy 1.8.2 (ref. 55; RRID:SCR\_018139; https://github.com/scverse/scanpy) was used to cluster the data in latent space using the leiden algorithm (56), and marker genes were identified in latent space using TotalVI.

#### CITE-seq Data Analysis

Clusters were annotated using clustifyr 1.9.1 (ref. 15; https:// github.com/rnabioco/clustifyr) and the leukemic/normal bone marrow reference dataset generated by Triana and colleagues (57). Scanpy and Seurat 4.1.1 (ref. 58; RRID:SCR\_007322, https://github. com/satijalab/seurat) were then used to generate uniform manifold approximation and projections from the TotalVI embeddings and perform exploratory analysis, data visualization, etc. The myeloid subpopulation in the CITE-seq data was reannotated using scArches 0.5.7 (ref. 17; https://github.com/theislab/scarches) and the leukemia reference dataset generated by Zeng and colleagues (14). The reference model was trained for 400 epochs based on the 3,000 most highly variable genes determined by scanpys' pp.highly\_variable\_ genes() function. Then the model was updated with transfer learning of the scArches algorithm to annotate the query myeloid subpopulation. CD34+\_LSCs and KMT2A-r\_LSCs were identified through scoring each individual cell using the AddModuleScore() function of the Seurat software and custom-generated candidate CD34+\_LSC and KMT2A-r\_LSC gene expression signatures, as stated in the main text.

### **WES Analysis**

WES libraries were generated using the Agilent SureSelect XT exome prep kit with 200 ng of input as per protocol (Agilent). The probe used was SureSelect XT Human All Exon V7 (Agilent). Libraries were normalized by Qubit (Invitrogen) and Tapestation (Agilent), and 2 × 150 bp reads were sequenced on a Novaseq 6000 (Illumina) to obtain 400× coverage. Fastqc v0.11.9 was used to assess overall sequencing quality, and reads were trimmed using cutadapt (cutadapt, RRID:SCR\_011841) v2.9 to remove the Illumina universal adapters, bases of poor quality (phred <30), and any reads in which the minimum read length was <10 base pairs in length.

Trimmed fastq files were then aligned to the GRCh38 p.13 genome using BWA v0.7.17 (BWA, RRID:SCR\_010910). Stringent quality control of alignments and read duplicate removal were performed using the Picard suite of tools v2.21.1 (Picard, RRID:SCR\_006525) and samtools v1.8 (samtools, RRID:SCR\_002105). Variants were called on alignments using DeepVariant v1.0.0, followed by BCFtools (BCFtools, RRID:SCR\_005227) v1.11 to filter variants of low quality. SNPs were removed if the raw unfiltered read depth was <20 reads and the mapping quality <30. All remaining variants were then annotated using Annovar v2020-06-07 (Annovar, RRID:SCR\_012821). Of all the databases that were used for annotations, the most notable ones used for data interpretation were the COSMIC database v92 (COSMIC, RRID:SCR\_002260), Clinvar v2020031 (Clinvar, RRID:SCR\_006169), SIFT (SIFT, RRID: SCR\_012813), PolyPhen (PolyPhen, RRID:SCR\_013189), and nci60. For comparing mutational profile between prim and mono cells, we focused on nonsynonymous exonic mutations that occurred in the 49 commonly mutated genes of AML.

### Metabolomic Analysis

For each Mono-AML specimen, five replicates of 500,000 cells each were freshly sorted from the m-LSC-enriched D subpopulation (CD34<sup>-</sup>, CD4<sup>+</sup>, CD14<sup>-</sup>, CD11b<sup>-</sup>, CD36<sup>-</sup> m-LSC) and the non-m-LSC E subpopulation (CD34<sup>-</sup>, CD4<sup>+</sup>, CD14<sup>-</sup>, CD11b<sup>+</sup>, CD36<sup>+</sup> non-m-LSC). Sorted cells were washed in ice-cold PBS, and the cell pellets were snap-frozen for ultra-high performance liquid chromatographymass spectrometry analysis as described previously (32). Results were normalized by cell number. Pathway enrichment analysis was performed on metabolites that were  $\geq$ 1.2-fold higher in population D compared with E and with a *P* value of less than 0.1. All analyses were performed using the MetaboAnalyst 5.0 software (MetaboAnalyst, RRID:SCR\_015539; https://www.metaboanalyst.ca/).

## Statistical Analysis

Statistical analyses were performed in GraphPad Prism 9.3.1 (GraphPad Prism, RRID:SCR\_002798). Median ± interquartile range was used to describe summary statistics. One-tailed or two-tailed Mann–Whitney tests were used to compare two groups when applicable. Kruskal–Wallis tests with correction for multiple comparisons using the original FDR method of Benjamini and Hochberg were used to compare three or more groups. The exact statistical analysis methods are provided in the figure legends.

#### Data Availability

The data that support the findings of this study are available from the corresponding author upon reasonable request. CITE-seq data are available in the Gene Expression Omnibus (GSE232559). WES data are available to qualified academic investigators upon request to the CU Anschutz Chief Research Informatics Officer, Dr. Melissa Haendel (CRIO@cuanschutz.edu). Approved requests will be forwarded via e-mail to Dr. Ian Brooks, Director of Health Data Compass (HealthDataCompass@ucdenver.edu), who will arrange encryption and transfer of data via appropriate methods such as sftp or cloud-cloud push/transfer.

#### Authors' Disclosures

A.E. Gillen reports grants from United States Department of Veterans Affairs outside the submitted work, as well as a patent for methods of treating AML pending. T.M. Brunetti reports personal fees from Pluto Biosciences outside the submitted work. C.M. McMahon reports other support from Arcellx and Kura outside the submitted work. C.A. Smith reports a patent for methods of treating AML pending, and is the Chief Medical Officer of OncoVerity and a consultant for AML JV. D.A. Pollyea reports grants and personal

fees from AbbVie, and personal fees from Genentech, Zentalis, and BeiGene outside the submitted work. C.T. Jordan reports a patent for methods of treating AML pending. No disclosures were reported by the other authors.

### **Authors' Contributions**

S. Pei: Conceptualization, resources, data curation, formal analysis, supervision, funding acquisition, validation, investigation, methodology, writing-original draft, project administration, writing-review and editing. I.T. Shelton: Conceptualization, formal analysis, funding acquisition, validation, investigation, methodology, writing-review and editing. A.E. Gillen: Conceptualization, data curation, formal analysis, supervision, validation, investigation, visualization, writingoriginal draft, writing-review and editing. B.M. Stevens: Conceptualization, resources, data curation, formal analysis, supervision, validation, investigation, visualization, writing-original draft, writingreview and editing. M. Gasparetto: Resources, formal analysis, supervision, validation, investigation, writing-review and editing. Y. Wang: Validation, investigation, writing-review and editing. L. Liu: Investigation, writing-review and editing. J. Liu: Investigation. T.M. Brunetti: Resources, investigation. K. Engel: Conceptualization, resources, formal analysis, investigation, writing-review and editing. S. Staggs: Conceptualization, resources, formal analysis, supervision, validation, investigation, writing-review and editing. W. Showers: Resources, supervision, validation, investigation, visualization, writing-review and editing. A.I. Sheth: Resources, investigation, visualization, writing-review and editing. M.L. Amaya: Investigation, writing-review and editing. M. Minhajuddin: Formal analysis, investigation, writingreview and editing. A. Winters: Resources, formal analysis, investigation, writing-review and editing. S.B. Patel: Resources, investigation. H. Tolison: Investigation, writing-review and editing. A.E. Krug: Investigation, writing-review and editing. T.N. Young: Investigation. J. Schowinsky: Investigation, methodology, writing-review and editing. C.M. McMahon: Investigation, methodology, writing-review and editing. C.A. Smith: Conceptualization, resources, supervision, investigation, methodology, writing-review and editing. D.A. Pollyea: Conceptualization, resources, supervision, funding acquisition, methodology, writing-review and editing. C.T. Jordan: Conceptualization, resources, data curation, formal analysis, supervision, funding acquisition, validation, investigation, methodology, writing-original draft, project administration, writing-review and editing.

## Acknowledgments

We thank all the patients and their families, as well as the nurses, pharmacists, and advanced practice practitioners who were involved in their care. S. Pei is generously supported by the National Natural Science Foundation of China (82270157) and grants from the Key Research and Development Program of Zhejiang (2022C03005). C.T. Jordan is generously supported by the Nancy Carroll Allen Chair in Hematology Research, a Leukemia & Lymphoma Society Specialized Center of Research Program grant (7020-19), NIH R35CA242376, and Veterans Administration merit award BX004768-01. A.E. Gillen is supported by the United States Department of Veterans Affairs (IK2BX004952-01A1). D.A. Pollyea is supported by the University of Colorado Department of Medicine Outstanding Early Career Scholar Program, the Robert H. Allen MD Chair in Hematology Research, and a Leukemia & Lymphoma Society Scholar in Clinical Research Award. A.I. Sheth is supported by an NCI National Research Service Award F30 grant (F30CA254251). M.L. Amaya is supported by the United States Department of Veterans Affairs Biomedical Laboratory R&D CDA-2. This study was also partly supported by NIH P30CA046934 Bioinformatics and Biostatistics Shared Resource through the University of Colorado Anschutz Medical Campus Cancer Center Bioinformatics Core Facility (RRID:SCR\_021983). We thank Dr. Ryan M. Layer for his help with WES analysis. We gratefully acknowledge

research support from the Colorado Nutrition Obesity Research Center (NIH P30 DK48520).

The publication costs of this article were defrayed in part by the payment of publication fees. Therefore, and solely to indicate this fact, this article is hereby marked "advertisement" in accordance with 18 USC section 1734.

#### Note

Supplementary data for this article are available at Cancer Discovery Online (http://cancerdiscovery.aacrjournals.org/).

Received November 15, 2022; revised April 21, 2023; accepted June 22, 2023; published first June 26, 2023.

#### **REFERENCES**

- Kreso A, Dick JE. Evolution of the cancer stem cell model. Cell Stem Cell 2014:14:275–91.
- Pollyea DA, Jordan CT. Therapeutic targeting of acute myeloid leukemia stem cells. Blood 2017;129:1627–35.
- Thomas D, Majeti R. Biology and relevance of human acute myeloid leukemia stem cells. Blood 2017;129:1577-85.
- Bonnet D, Dick JE. Human acute myeloid leukemia is organized as a hierarchy that originates from a primitive hematopoietic cell. Nat Med 1997;3:730-7.
- Hope KJ, Jin L, Dick JE. Acute myeloid leukemia originates from a hierarchy of leukemic stem cell classes that differ in self-renewal capacity. Nat Immunol 2004;5:738–43.
- Sarry JE, Murphy K, Perry R, Sanchez PV, Secreto A, Keefer C, et al. Human acute myelogenous leukemia stem cells are rare and heterogeneous when assayed in NOD/SCID/IL2Rgammac-deficient mice. J Clin Invest 2011;121:384–95.
- Ho TC, LaMere M, Stevens BM, Ashton JM, Myers JR, O'Dwyer KM, et al. Evolution of acute myelogenous leukemia stem cell properties after treatment and progression. Blood 2016;128:1671–8.
- Quek L, Otto GW, Garnett C, Lhermitte L, Karamitros D, Stoilova B, et al. Genetically distinct leukemic stem cells in human CD34-acute myeloid leukemia are arrested at a hemopoietic precursor-like stage. I Exp Med 2016:213:1513-35.
- Goardon N, Marchi E, Atzberger A, Quek L, Schuh A, Soneji S, et al. Coexistence of LMPP-like and GMP-like leukemia stem cells in acute myeloid leukemia. Cancer Cell 2011;19:138–52.
- Miles LA, Bowman RL, Merlinsky TR, Csete IS, Ooi AT, Durruthy-Durruthy R, et al. Single-cell mutation analysis of clonal evolution in myeloid malignancies. Nature 2020;587:477–82.
- Morita K, Wang F, Jahn K, Hu T, Tanaka T, Sasaki Y, et al. Clonal evolution of acute myeloid leukemia revealed by high-throughput single-cell genomics. Nat Commun 2020;11:5327.
- Pei S, Pollyea DA, Gustafson A, Stevens BM, Minhajuddin M, Fu R, et al. Monocytic subclones confer resistance to venetoclax-based therapy in patients with acute myeloid leukemia. Cancer Discov 2020;10:536–51.
- Bennett JM, Catovsky D, Daniel MT, Flandrin G, Galton DA, Gralnick HR, et al. Proposals for the classification of the acute leukaemias. French-American-British (FAB) co-operative group. Br J Haematol 1976;33: 451.8
- Zeng AGX, Bansal S, Jin L, Mitchell A, Chen WC, Abbas HA, et al. A cellular hierarchy framework for understanding heterogeneity and predicting drug response in acute myeloid leukemia. Nat Med 2022;28: 1212–23.
- Fu R, Gillen AE, Sheridan RM, Tian C, Daya M, Hao Y, et al. clustifyr: an R package for automated single-cell RNA sequencing cluster classification. F1000Res. 2020;9:223.
- Novershtern N, Subramanian A, Lawton LN, Mak RH, Haining WN, McConkey ME, et al. Densely interconnected transcriptional circuits control cell states in human hematopoiesis. Cell 2011;144:296–309.
- Lotfollahi M, Naghipourfar M, Luecken MD, Khajavi M, Buttner M, Wagenstetter M, et al. Mapping single-cell data to reference atlases by transfer learning. Nat Biotechnol 2022;40:121–30.

- Somervaille TC, Cleary ML. Identification and characterization of leukemia stem cells in murine MLL-AF9 acute myeloid leukemia. Cancer Cell 2006;10:257–68.
- Somervaille TC, Matheny CJ, Spencer GJ, Iwasaki M, Rinn JL, Witten DM, et al. Hierarchical maintenance of MLL myeloid leukemia stem cells employs a transcriptional program shared with embryonic rather than adult stem cells. Cell Stem Cell 2009;4:129-40.
- Hess JL, Bittner CB, Zeisig DT, Bach C, Fuchs U, Borkhardt A, et al. c-Myb is an essential downstream target for homeobox-mediated transformation of hematopoietic cells. Blood 2006;108:297–304.
- Krivtsov AV, Twomey D, Feng Z, Stubbs MC, Wang Y, Faber J, et al. Transformation from committed progenitor to leukaemia stem cell initiated by MLL-AF9. Nature 2006;442:818–22.
- Schoch C, Schnittger S, Klaus M, Kern W, Hiddemann W, Haferlach T. AML with 11q23/MLL abnormalities as defined by the WHO classification: incidence, partner chromosomes, FAB subtype, age distribution, and prognostic impact in an unselected series of 1897 cytogenetically analyzed AML cases. Blood 2003;102:2395–402.
- Iwasaki M, Liedtke M, Gentles AJ, Cleary ML. CD93 marks a nonquiescent human leukemia stem cell population and is required for development of MLL-rearranged acute myeloid leukemia. Cell Stem Cell 2015;17:412–21.
- Ng SW, Mitchell A, Kennedy JA, Chen WC, McLeod J, Ibrahimova N, et al. A 17-gene stemness score for rapid determination of risk in acute leukaemia. Nature 2016;540:433–7.
- Eppert K, Takenaka K, Lechman ER, Waldron L, Nilsson B, van Galen P, et al. Stem cell gene expression programs influence clinical outcome in human leukemia. Nat Med 2011;17:1086-93.
- Kozminski P, Halik PK, Chesori R, Gniazdowska E. Overview of dualacting drug methotrexate in different neurological diseases, autoimmune pathologies and cancers. Int J Mol Sci 2020;21:3483.
- Sykes DB, Kfoury YS, Mercier FE, Wawer MJ, Law JM, Haynes MK, et al. Inhibition of dihydroorotate dehydrogenase overcomes differentiation blockade in acute myeloid leukemia. Cell 2016;167:171–86.
- Sigal DS, Miller HJ, Schram ED, Saven A. Beyond hairy cell: the activity of cladribine in other hematologic malignancies. Blood 2010;116: 2884-96.
- Pabst C, Bergeron A, Lavallee VP, Yeh J, Gendron P, Norddahl GL, et al. GPR56 identifies primary human acute myeloid leukemia cells with high repopulating potential in vivo. Blood 2016;127:2018–27.
- Waclawiczek A, Leppa AM, Renders S, Stumpf K, Reyneri C, Betz B, et al. Combinatorial BCL2 family expression in acute myeloid leukemia stem cells predicts clinical response to azacitidine/venetoclax. Cancer Discov 2023;13:1408–27.
- Pollyea DA, Stevens BM, Jones CL, Winters A, Pei S, Minhajuddin M, et al. Venetoclax with azacitidine disrupts energy metabolism and targets leukemia stem cells in patients with acute myeloid leukemia. Nat Med 2018;24:1859–66.
- Jones CL, Stevens BM, Pollyea DA, Culp-Hill R, Reisz JA, Nemkov T, et al. Nicotinamide metabolism mediates resistance to venetoclax in relapsed acute myeloid leukemia stem cells. Cell Stem Cell 2020;27:748–64.
- Jones CL, Stevens BM, D'Alessandro A, Reisz JA, Culp-Hill R, Nemkov T, et al. Inhibition of amino acid metabolism selectively targets human leukemia stem cells. Cancer Cell 2018;34:724–40.
- Jones CL, Inguva A, Jordan CT. Targeting energy metabolism in cancer stem cells: progress and challenges in leukemia and solid tumors. Cell Stem Cell 2021;28:378-93.
- Stevens BM, Jones CL, Pollyea DA, Culp-Hill R, D'Alessandro A, Winters A, et al. Fatty acid metabolism underlies venetoclax resistance in acute myeloid leukemia stem cells. Nat Cancer 2020;1:1176–87.
- Ye H, Adane B, Khan N, Sullivan T, Minhajuddin M, Gasparetto M, et al. Leukemic stem cells evade chemotherapy by metabolic adaptation to an adipose tissue niche. Cell Stem Cell 2016;19:23–37.
- DiNardo CD, Lachowiez CA, Takahashi K, Loghavi S, Xiao L, Kadia T, et al. Venetoclax combined with FLAG-IDA induction and consolidation in newly diagnosed and relapsed or refractory acute myeloid leukemia. J Clin Oncol 2021;39:2768–78.
- 38. Kadia TM, Reville PK, Borthakur G, Yilmaz M, Kornblau S, Alvarado Y, et al. Venetoclax plus intensive chemotherapy with cladribine,

- idarubicin, and cytarabine in patients with newly diagnosed acute myeloid leukaemia or high-risk myelodysplastic syndrome: a cohort from a single-centre, single-arm, phase 2 trial. Lancet Haematol 2021;8: e552–e61.
- Kadia TM, Reville PK, Wang X, Rausch CR, Borthakur G, Pemmaraju N, et al. Phase II study of venetoclax added to cladribine plus low-dose cytarabine alternating with 5-azacitidine in older patients with newly diagnosed acute myeloid leukemia. J Clin Oncol 2022;40:3848–57.
- 40. Wang H, Mao L, Yang M, Qian P, Lu H, Tong H, et al. Venetoclax plus 3 + 7 daunorubicin and cytarabine chemotherapy as first-line treatment for adults with acute myeloid leukaemia: a multicentre, single-arm, phase 2 trial. Lancet Haematol 2022;9:e415–e24.
- Zainaldin C, Arora S, Bathini S, Gupta U, Pandya V, Bae S, et al. Dismal survival outcomes of patients with acute myeloid leukemia after failure of venetoclax with hypomethylating agents. Leuk Lymphoma 2022;63: 3245–8.
- Maiti A, Rausch CR, Cortes JE, Pemmaraju N, Daver NG, Ravandi F, et al. Outcomes of relapsed or refractory acute myeloid leukemia after frontline hypomethylating agent and venetoclax regimens. Haematologica 2021;106:894–8.
- Zhang H, Nakauchi Y, Kohnke T, Stafford M, Bottomly D, Thomas R, et al. Integrated analysis of patient samples identifies biomarkers for venetoclax efficacy and combination strategies in acute myeloid leukemia. Nat Cancer 2020;1:826–39.
- Cozzio A, Passegue E, Ayton PM, Karsunky H, Cleary ML, Weissman IL. Similar MLL-associated leukemias arising from self-renewing stem cells and short-lived myeloid progenitors. Genes Dev 2003;17:3029–35.
- Zeisig BB, Fung TK, Zarowiecki M, Tsai CT, Luo H, Stanojevic B, et al. Functional reconstruction of human AML reveals stem cell origin and vulnerability of treatment-resistant MLL-rearranged leukemia. Sci Transl Med 2021;13:eabc4822.
- DiNardo CD, Tiong IS, Quaglieri A, MacRaild S, Loghavi S, Brown FC, et al. Molecular patterns of response and treatment failure after frontline venetoclax combinations in older patients with AML. Blood 2020;135: 791–803
- Ganan-Gomez I, Yang H, Ma F, Montalban-Bravo G, Thongon N, Marchica V, et al. Stem cell architecture drives myelodysplastic syndrome progression and predicts response to venetoclax-based therapy. Nat Med 2022;28:557–67.
- Pei S, Minhajuddin M, Adane B, Khan N, Stevens BM, Mack SC, et al. AMPK/FIS1-mediated mitophagy is required for self-renewal of human AML stem cells. Cell Stem Cell 2018;23:86–100.
- Dobin A, Davis CA, Schlesinger F, Drenkow J, Zaleski C, Jha S, et al. STAR: ultrafast universal RNA-seq aligner. Bioinformatics 2013;29:15–21.
- Xin H, Lian Q, Jiang Y, Luo J, Wang X, Erb C, et al. GMM-Demux: sample demultiplexing, multiplet detection, experiment planning, and novel cell-type verification in single cell sequencing. Genome Biol 2020;21:188.
- Heiser CN, Wang VM, Chen B, Hughey JJ, Lau KS. Automated quality control and cell identification of droplet-based single-cell data using dropkick. Genome Res 2021;31:1742–52.
- Yang S, Corbett SE, Koga Y, Wang Z, Johnson WE, Yajima M, et al. Decontamination of ambient RNA in single-cell RNA-seq with DecontX. Genome Biol 2020;21:57.
- McGinnis CS, Murrow LM, Gartner ZJ. DoubletFinder: doublet detection in single-cell RNA sequencing data using artificial nearest neighbors. Cell Syst 2019;8:329–37.
- Gayoso A, Steier Z, Lopez R, Regier J, Nazor KL, Streets A, et al. Joint probabilistic modeling of single-cell multi-omic data with totalVI. Nat Methods 2021;18:272–82.
- Wolf FA, Angerer P, Theis FJ. SCANPY: large-scale single-cell gene expression data analysis. Genome Biol 2018;19:15.
- Traag VA, Waltman L, van Eck NJ. From Louvain to Leiden: guaranteeing well-connected communities. Sci Rep. 2019;9:5233.
- Triana S, Vonficht D, Jopp-Saile L, Raffel S, Lutz R, Leonce D, et al. Single-cell proteo-genomic reference maps of the hematopoietic system enable the purification and massive profiling of precisely defined cell states. Nat Immunol 2021;22:1577–89.
- Hao Y, Hao S, Andersen-Nissen E, Mauck WM 3rd, Zheng S, Butler A, et al. Integrated analysis of multimodal single-cell data. Cell 2021;184:3573–87.